Cesium-metalloid halide perovskites MBX$_3$ (M^{1+} = Cs; B^{2+} = Si, Ge, Sn, Pb; X$^−$ = Cl, Br, I) as semiconductor photovoltaic materials for sustainable renewable-energy applications

A. Almeshal [a], M. Musa Saad H.-E. [a,*], B. O. Alsobhi [b]
[a]Department of Physics, College of Science and Arts in Al-Muthnib, Qassim University, Al-Muthnib 51931, Saudi Arabia
[b]Physics Department, Faculty of Science, Taibah University, Al-Madinah al-Munawarah, Saudi Arabia

With the dawning of 21st century, governments faced three urgent challenges, global economic crisis, energy crisis and global warming. So, the research goals have directed on developing novel renewable-energy technologies as suitable alternative sources of the traditional energy that addresses these problems. Photovoltaic based solar cells technology gives sustainable solutions and depends on inorganic materials with specific properties. Among this family, halide perovskites (MBX$_3$) have been investigated during the last five years. Besides studying their unique properties as flexible structures, high stability, tunable semiconductor band-gap (E$_g$ < 2.50 eV), high charge-carrier mobility and large optical absorption, research also seek for promising and multifaceted electroptical applications that give an amazing power efficiency (~24.0 %) in photovoltaic technology. The current challenge is to synthesis MBX$_3$ materials provide suitable properties, include notable chemical stability at high temperatures, high electrical power efficiency, broad emission and tunable semiconducting E$_g$. Motivated by the site substitution effect, we extended this concept to build a series of cesium-metalloid MBX$_3$ (M^{1+} = Cs; B^{2+} = Si, Ge, Sn, Pb; X$^−$ = Cl, Br, I), and investigate their structural, stability and optoelectronic properties. We expect these investigations will provide inspiration for an innovation of such MBX$_3$ materials in photovoltaic applications.

1. Introduction

Currently, world's population and government officials face urgent challenges represented by the economic collapse, traditional fuel crisis, global warming and environment problems. Therefore, intensive efforts have been directed by scientists to find effective and rapid solutions to these challenges, especially the energy crisis. Also, to provide a sustainable solution to the problem of increasing demand for cheap and clean energy sources, research interest has focused on developing novel electrical sources that serve renewable energy technology. They are considered as appropriate and alternative sources instead of traditional energy sources, fossil fuels which exhaust economy and their emissions cause global warming [1-3]. For these reasons, it is an essential requirement to develop alternative energy technologies that preserve the local economies, environment and public health. Amongst, photovoltaics (PV) based solar cells technology is sustainable solution and offers a set of benefits, such as it helps prevent the global warming and protects the environmental, reduces the financial spending on energy manufacture, and supports the local economies [1,4]. The manufacturing process of photovoltaic PV solar cells depends chiefly on certain organic-inorganic, mixed organic and pure inorganic materials having specific physical and chemical characteristics.

During the last five years, various materials, among this family, consist of complete inorganic metal halide perovskite compounds (chemical formula MBX_3) have been produced and investigated their properties in detail. Many research studies have mainly to investigate the unique characteristics of MBX_3 materials, such as flexible crystal structure, high structural stability, tunable semiconducting band gap, high mobility of charge carrier and great optical absorption [5-8]. In addition, research works within these MBX_3 compounds search for multi-faceted and promising electroptical and thermoptical applications provide remarkable efficiency of power conversion process. The above characteristics make halide perovskite compounds promising materials for photovoltaics PV solar cells technology [9-16]. The recent challenge is the synthesis of novel MBX_3 materials that have distinct properties and are suitable for photovoltaics PV applications. Various properties have reported in some halide perovskite semiconductors MBX_3 materials, such as notable structural stability at high temperature ranges, tunable band gap, high electrical efficiency of power conversion, broad optical absorption and large emission [17].

In this research work, motivated by the effect of M, B and B sites replacement on properties of MBX_3, we have extended this concept to build a series of related inorganic halide perovskites MBX_3. Besides examining the effect of site substitution (M^{1+} = Cs; B^{2+} = Si, Ge, Sn, Pb; X^- = Cl, Br, I), we investigated the structural, electronic and optical properties of these materials. Several theoretical and experimental researches have been carried out on cubic compounds in MBX_3 family by replacing M, B and X sites with three different atoms. The cubic structure (Pm-3m; #221) is the majority crystal symmetry in solid state physics, solid state chemistry and materials science. Thus, due to the complete possibility of replacement the three atoms in M, B and X positions of parent compound MBX_3 by suitable metal, metalloid and halogen atoms, respectively, these halide perovskites MBX_3 can offer numerous multifunctional properties make them promising candidate materials for novel photovoltaic PV, solar cells, optoelectronic and other technologies [18-20]. Thus, certain compounds with MBX_3 structure can provided amazing performances in many future fields of materials applications such as in photovoltaics PV, solar cells technology [1], memory devices, sensors tools, diode apparatus [3,7], electrodes equipment [19]. Also, they show properties suitable for classical applications; piezoelectricity, ferroelectricity, superconductivity and so on [14]. The above properties and applications have attracted the attention of scientists, researchers and engineering to devote colossal efforts on metal halide perovskites MBX_3 materials to investigate and discover novel and functional properties for future applications [5,12,15,18].

The main objective of the present study is to search for tunable semiconductor materials among the complete metal halide perovskite MBX_3. To achieve this goal, we investigate the chemical structure and physical properties of a series contain twelve related compounds of metal-metalloid halide perovskite MBX_3. Three sites of MBX_3 are selected as: M is an alkali-metal, i.e. Cesium atom (M = Cs^{1+}), B is metalloid and post-transition atoms (B = Si^{2+}, Ge^{2+}, Sn^{2+}, Pb^{2+}) and X is a halogen atom (X = Cl^-, Br^-, I^-). This paper presents detailed results of halide perovskites, which have not been predicted theoretically and experimentally, and could be contribution to the novel materials science for the development these compounds with desirable properties. Our contribution and main goal in this domain is to examine the effect of site substitution in B^{2+} and X^- positions (B = Si^{2+}, Ge^{2+}, Sn^{2+}, Pb^{2+}) and (X = Cl^-, Br^-, I^-), respectively, on the structural and electroptical properties of MBX_3. The key purpose of selecting of metalloid and post-transition atoms, Silicon (Si), Germanium (Ge), Tin (Sn) and Lead (Pb), in this series is due to their similar electronic configuration of 5s and 5p orbitals. Si (Z = 14; [Ne] $3s^2$ $3p^2$), Ge (Z = 32; [Ar] $3d^{10}$ $4s^2$ $4p^2$), Sn (Z = 50; [Kr] $4d^{10}$ $5s^2$ $5p^2$) and Pb (Z = 82; [Xe] $5d^{10}$ $6s^2$ $6p^2$). Also, these atoms share amalgamated position within the p-block, in group XIV of the international Periodic Table of elements.

In this study, we will provide first-principles density functional theory (DFT) bases to recognize the physical properties of inorganic halide perovskites MBX_3 (M^{1+} = Cs; B^{2+} = Si, Ge, Sn, Pb; X^- = Cl, Br, I) and their dependence on the nature of B^{2+} and X^- sites. Here, all DFT investigations were performed by using the generalized gradient approximation (GGA-PBE), to investigate the structural, electronic and optical properties of MBX_3. As a result of these DFT investigations and based on the obtained properties, we expect that these halide perovskite

semiconductors MBX_3 can be candidate materials for photovoltaics PV, solar cells, photodiodes, photodetectors and new related applications.

2. Calculations methods

First-principles density functional theory (DFT) [21] investigations are used to find out the ground states and physical properties of the studied compounds of Ce-based halide perovskites MBX_3 (M^{1+} = Cs; B^{2+} = Si, Ge, Sn, Pb; X^- = Cl, Br, I). The calculations are carried out by using the wonderful computational capabilities of the 2019 version of Wien2k package [22]. Wien2k code utilizes the method of full-potential linearized augmented plane-wave (FPLAPW) based on Kohn-Sham (KS) methodology [23]. Further, the Perdew-Burke-Ernzerhof functional [24] within FPLAPW which employ the generalized gradient approximation (PBE-GGA) method [27] is used to modulate the chemical structures and physical properties of these MBX_3 materials. We also performed non spin-polarized version of DFT calculations to acquire the appropriate results of these properties. In PFLAPW approximation, the crystal space of the MBX_3 unit cell contains two major regions; the first region of which is a spherical region or muffin-tin (MT) region, hence the local potential is likely to be have spherical symmetry. The spherical region is specified by the values of muffin-tin radii R_{MT} as ($r \leq R_{MT}$). In DFT calculations, the muffin-tin radii R_{MT} for the individual atoms in MBX_3, i.e. M, B and X, are selected differently as follow: [R_{MT} (M) = 2.2 a.u., R_{MT} (B) = 2.0 a.u. and R_{MT} (X) = 1.8 a.u.]. Here, the solution of the Schrödinger equation (SE) is described by multiplying radial function and spherical harmonic in this region of muffin-tin MT. The second region outside muffin-tin atoms or interstitial region (IR) in which the electric potential value is believed to be constant ($r > R_{MT}$), and its Schrödinger equation SE is solved by plane wave function (PLW). The ground state energy per unit cell of MBX_3 is obtained by setting the convergence criteria as (ε = 0.0001 Ry) and charge density as (ρ = 0.001 e). The total number of (k_{points} = 1000) in the first Brillouin zone (BZ) with a cutoff value ($R_{MT}K_{max}$ = 8.0) have been opened. R_{MT} refers to the smallest muffin-tin MT radius whereas K_{max} represents the largest reciprocal lattice vector [22]. The structural optimizations of halide perovskites MBX_3 are performed as an initial step; the energy per unit cell (E) has been calculated as a function of the variation of unit cell volume (V).

3. Results and discussion

3.1. Structural optimization properties

As a first stage, the structural optimizations for all compounds of halide perovskites MBX_3 (M^{1+} = Cs; B^{2+} = Si, Ge, Sn, Pb; X^- = Cl, Br, I) are carried out by using the practical capabilities of GGA-PBE method based on the Wien2k code. Then, we extracted the equilibrium results of structural parameters like ground state energy (E_0), unit cell volume (V_0), lattice constants (a_0), bulk modulus (B), and first pressure derivative of bulk modulus B (B'). All these results of MBX_3 are expected by fitting the variation of the total energy (E^{Tot}) per unit cell as a function of the corresponding unit cell volume (V^{Cell}), as expressed by the Murnaghan's equation of state:

$$E^{Tot} - E_0 = \frac{B_0 V^{Cell}}{B_0'} - \frac{B_0 V_0}{(B_0' - 1)} + \frac{B_0 V^{Cell}}{B_0'} \frac{(V_0/V^{Cell})^{B_0'}}{(B_0' - 1)} \tag{1}$$

Figs. 1-4 show the obtained curves of total energy (E) versus unit cell volume (V) for the structures of halide perovskites MBX_3 optimized by using the PBE method within PBE-GGA method. From these (E vs. V) optimizations curves we extracted the structural parameters of MBX_3 and summarized them in (Table 1). Accordingly, we can conclude that all compounds of MBX_3 show nonmagnetic (NM) state. Also, we can see that the value of lattice constant a_0 increases with the increase in the number of valence electrons per unit cell for MBX_3. Thus, the atomic number of the two cations (M^{1+} = Cs) and (B^{2+} = Si, Ge, Sn, Pb), and anion (X^- = Cl, Br, I)

have major effect on these results. The enhancement in values of lattice constant a_0 of MBX$_3$ is due principally to the increase in atomic radii and electronic charges of p-block cation B^{2+} starting from (B = Si; Z = 14) to (B = Ge; Z = 32) to (B = Sn; Z = 50) to (B = Pb; Z = 82). Similar trend have been distinguished in previous reports of theoretical DFT studies on analogous halide perovskites MBX$_3$, where (M^{1+} = K, Rb, Cs; B^{2+} = Ge, Sn; X$^-$ = Cl, Br, I) [28,29].

In addition, it can see that the value of bulk modulus B decreases sequentially ($B_{Si} > B_{Ge} > B_{Sn} > B_{Pb}$) by changing the B^{2+} atom in unit cell of MBX$_3$, see (Table 1). The obtained results of bulk modulus B also confirm that there is enhancement in the values of stiffness properties for MBX$_3$ structures. This indicates that more rigidity and less compressible properties can be got by changing the B^{2+} atom within the series (B^{2+} = Ge, Sn, Pb). The present calculations are in a good agreement with the previous PBE-GGA reports that have studied similar metal-based halide perovskite semiconductors MBX$_3$ with (M^{1+} = K, Rb, Cs; B^{2+} = Ge; X$^-$ = F, Cl, Br) [29]. Furthermore, we display the results of optimized atomic distances and positions in the cubic structure of unit cell for halide perovskites MBX$_3$ (from Fig. 5) respectively in Tables 2 and 3.
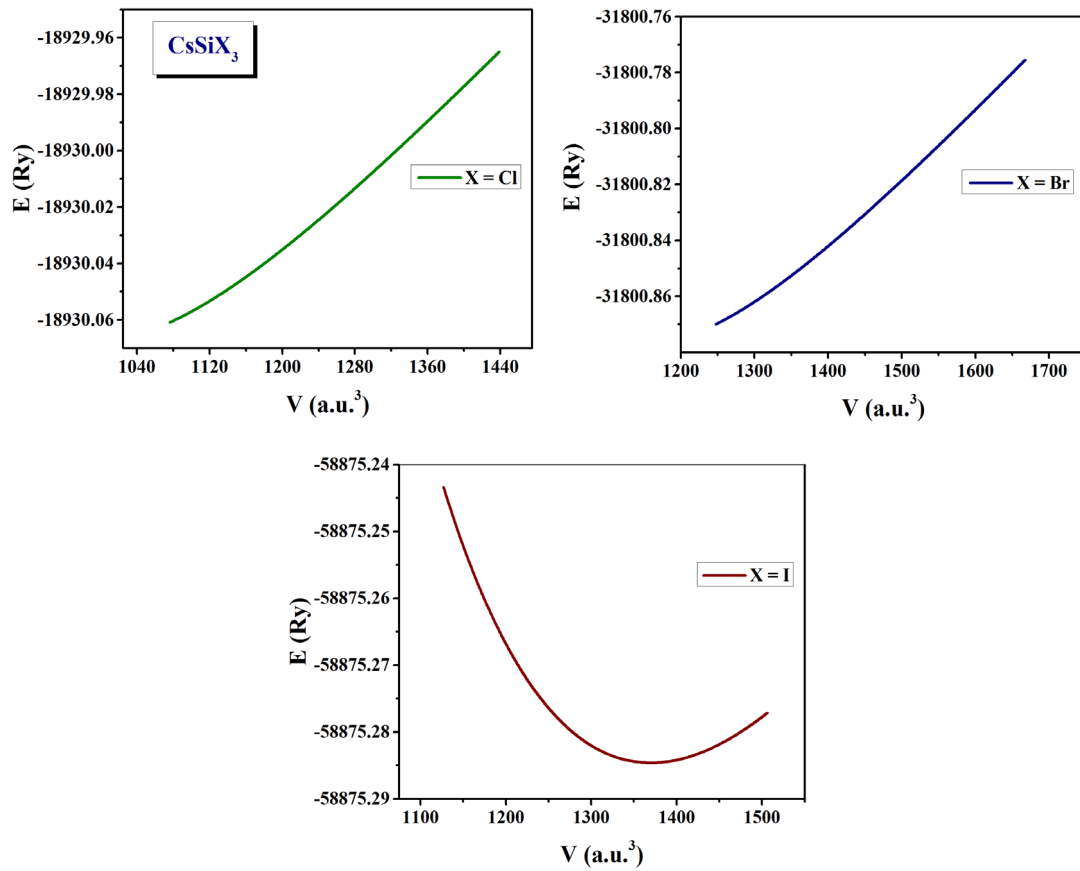

Fig. 1. Total energy (E) as a function of unit cell volume (V) of CsSiX$_3$ (X = Cl, Br, I).
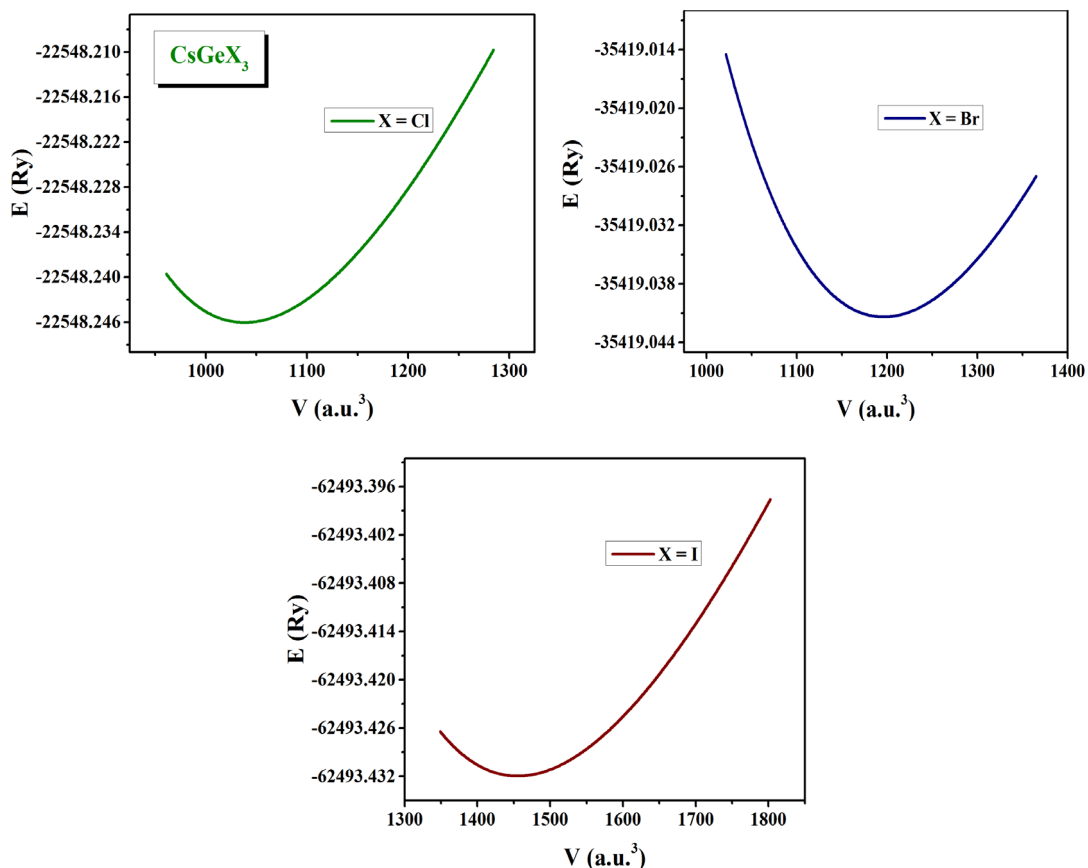
Fig. 2. Total energy (E) as a function of unit cell volume (V) of CsGeX$_3$ (X = Cl, Br, I).
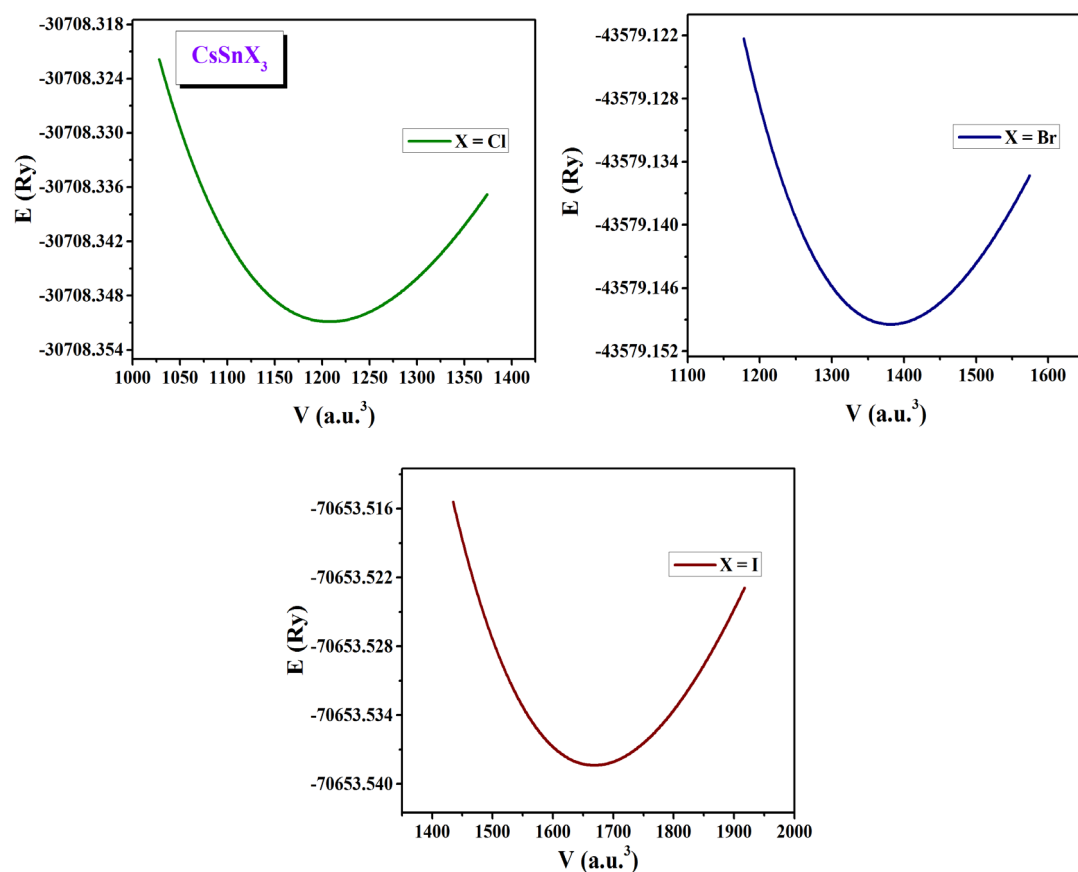
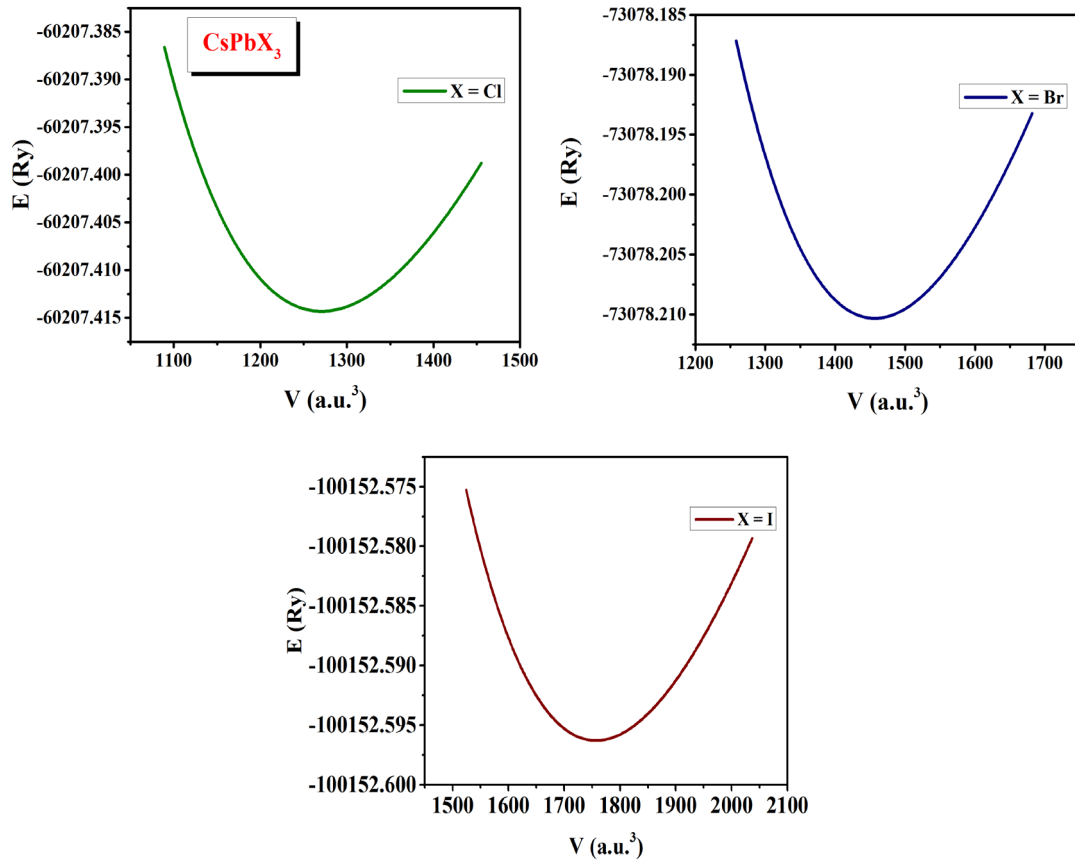*Fig. 3. Total energy (E) as a function of unit cell volume (V) of CsSnX$_3$ (X = Cl, Br, I).*

Fig. 4. Total energy (E) as a function of unit cell volume (V) of (X = Cl, Br, I).

Table 1. The structural parameters of the unit cell for the halide perovskites MBX_3 (M^{1+} = Cs; B^{2+} = Si, Ge, Sn, Pb; X^- = Cl, Br, I).

MBX_3 compound	a_0 (Å)	V_0 (Å^3)	B (GPa)	B' (GPa)
CsSiCl$_3$	5.246	144.4	28.06	4.211
CsSiBr$_3$	5.497	166.1	23.75	4.278
CsSiI$_3$	5.877	203.0	19.29	4.917
CsGeCl$_3$	5.359	153.9	27.73	4.729
CsGeBr$_3$	5.617	177.3	22.88	4.8036
CsGeI$_3$	5.997	215.7	17.90	4.2721
CsSnCl$_3$	5635	179.0	23.27	4.9250
CsSnBr$_3$	5.894	204.7	19.72	4.6468
CsSnI$_3$	6.277	247.3	15.72	4.3785
CsPbCl$_3$	5.732	188.3	22.64	5.3110
CsPbBr$_3$	5.999	215.9	19.05	4.7705
CsPbI$_3$	6.386	260.4	15.04	5.0021

Table 2. The optimized atomic distances in the unit cell of halide perovskites MBX₃
(M^{1+} = Cs; B^{2+} = Si, Ge, Sn, Pb; X^- = Cl, Br, I).

MBX₃ compound	Cs^+–B^{3+} (Å)	Cs^+–X^- (Å)	B^{2+}–X^- (Å)
CsSiCl₃	4.543	3.709	2.623
CsSiBr₃	4.769	3.887	2.749
CsSiI₃	5.090	4.156	2.938
CsGeCl₃	4.641	3.790	2.680
CsGeBr₃	4.865	3.972	2.809
CsGeI₃	5.194	4.241	2.999
CsSnCl₃	4.880	3.985	2.818
CsSnBr₃	5.104	4.168	2.947
CsSnI₃	5.436	4.438	3.138
CsPbCl₃	4.964	4.053	2.866
CsPbBr₃	5.195	4.242	2.999
CsPbI₃	5.530	4.515	3.193

Table 3. The atomic sites, Wyckoff positions and coordinates (x, y, z) in the cubic unit cell
(Pm-3m; Z = 2) of the halide perovskites MBX₃ (M^{1+} = Cs; B^{2+} = Si, Ge, Sn, Pb; X^- = Cl, Br, I).

Site	Wyckoff position	Atomic coordinates		
		x	y	z
M^{1+}-cation	1a	0	0	0
B^{2+}-cation	1b	½	½	½
X^--anion	3d	½	0	0
		0	½	0
		0	0	½

3.2. Structural stability properties

Halide perovskite compounds MBX₃ share two essential properties that decide their suitability as viable materials for photovoltaic PV solar cells applications: stability and efficiency. In order to estimate the crystallographic stability of the individual materials that composed the halide perovskites MBX₃ (M^{1+} = Cs; B^{2+} = Si, Ge, Sn, Pb; X^- = Cl, Br, I), the empirical criterion is accepted by calculating the tolerance factor (T_F) of these crystals [35]. The ration of tolerance factor T_F can be calculated through the geometric equation:

$$T_F = 0.707 \frac{(R_M + R_X)}{(R_B + R_X)} \tag{2}$$

where, R_M, R_B and R_X represent the ionic radii of atoms (M^{1+} = Cs), (B^{2+} = Si, Ge, Sn, Pb) and (X^- = Cl, Br, I) in crystal structures of MBX₃, respectively. We used the values R_M^{1+} = 2.02 Å (M^{1+} = Cs) in the XII-coordinate arrangement, R_B^{2+} = 0.64 Å (B^{2+} = Si), R_B^{2+} = 0.87 Å (B^{2+} = Ge), R_B^{2+} = 0.89 Å (B^{2+} = Sn) and R_B^{2+} = 0.92 Å (B^{2+} = Pb), and R_X^- = 1.67 Å (X^- = Cl), R_X^- = 1.82 Å (X^- = Br) and R_X^- = 2.06 Å (X^- = I), in the VI-coordinate arrangement [36].

In general, the ration value of tolerance factor T_F takes fluctuating values around the ideal value (T_F = 1.0) and it depends on to the size of atoms M, B and X that makeup the compound of perovskite MBX₃. A deviation of tolerance factor T_F value from the ideal T_F = 1.0 can be a measure of mismatch of the crystal structure perovskite MBX₃. This mismatch appears because there is small difference in the ionic radii, R_M^{1+}, R_B^{2+} and R_X^-, of the component atoms M^{1+}, B^{2+} and X^-, respectively. Frequently, the distortion in crystal structure of MBX₃ is escorted by mechanical compression and tension in the internal bonds of MBX₃, (M^{1+}– X^-) and (B^{2+}– X^-), due to the difference that recompensed by the crystal rotation and tilting in MX₆ and BX₆ octahedra [29]. As a result, the structural symmetry of perovskite MBX₃ lowers from the cubic structure

(Pm-3m; #221) causing a small deviation of the core angle in MBX$_3$ from the ideal (B$^+$–X$^-$–B$^+$ = 180˚). Thus, four general canons for such halide perovskites MBX$_3$ can be adopted; (0.980 < T$_F$ < 1.01) confirms the cubic structure (Pm-3m) and is the most probable. (T$_F$ > 1.110) validate for hexagonal symmetry (P6$_3$/mmc) in MBX$_3$ structure, and (0.97 < T$_F$ < 1.05) predicts the tetragonal symmetry (*I*4/m). While, (T$_F$ < 0.97) indicates that the compound of MBX$_3$ crystallizes in orthorhombic symmetry (Pnma; Pbnm) or in monoclinic structure (P2$_1$/n) [29,37-41]. From the above cases, it can see that the studied compounds of halide perovskites MBX$_3$ show values of tolerance factor T$_F$ match with the cubic Pm-3m symmetry (Table 4). The minor variations in these values are due to the small difference in the ionic radius of B^{2+} atoms (R$_B$$^{2+}$).

Also, there is an additional factor can used to measure the stability of crystal structure for halide perovskites MBX$_3$, i.e. octahedral factor (O_F). This factor can be applied to estimate the fitting of the B^{2+}-cations into their octahedra network [B^{2+}X$_6$]. It can be evaluated via the ratio between the ionic radii of the cations B^{2+} (B^{2+} = Si, Ge, Sn, Pb) and anions X$^-$ (X$^-$ = Cl, Br, I) in their corresponding bonds (B^{2+}– X$^-$) [38,41], as follow:

$$O_F = \frac{R_{B^{2+}}}{R_{X^-}} \times 100\% \tag{3}$$

From the calculated values of this octahedral factor O_F, as displayed in (Table 4), we note that all crystal structures of halide perovskites MBX$_3$ show more stability properties. This is because the values of the octahedral factor O_F are within the stability range (O_F = 44% − 90%) [38,41].

3.3. Thermodynamic stability properties

Formation energy (ΔE_F), which represent the chemical energy required to dissociate the solid compounds into their individual elements, is a useful factor that can measure the thermodynamic stability of these materials. Also, the formation energy ΔE_F examines the strength of internal bonding in crystal structures. Here, we calculated the formation energy ΔE_F of the studied compounds of halide perovskites MBX$_3$ (M^{1+} = Cs; B^{2+} = Si, Ge, Sn, Pb; X$^-$ = Cl, Br, I). The value of formation energy ΔE_F is calculated through the energy difference (ΔE) between the value of energy per unit cell MBX$_3$ and the value of energy per atom of three constructed atoms, M^{1+}, B^{2+} and X$^-$. The following equation calculates this energy [29,42]:

$$\Delta E_F = \frac{1}{\alpha + \beta + \gamma}\left[\left(E_{MBX_3}^{Total}\right) - \left(\alpha E_M^{(s)} + \beta E_B^{(s)} + \gamma E_X^{(s)}\right)\right] \tag{4}$$

where, $E_{MBX_3}^{Total}$ stands for the total energy per unit cell of MBX$_3$, and $E_M^{(s)}$, $E_B^{(s)}$ (B^{2+} = Si, Ge, Sn, Pb) and $E_X^{(s)}$ (X$^-$ = Cl, Br, I) denote the partial chemical energies of the individual atoms in solid state phase (s) in the unit cell. The integer values α, β and γ represent the numbers of the atoms M^{1+}, B^{2+} (B^{2+} = Si, Ge, Sn, Pb) and X$^-$ (X$^-$ = Cl, Br, I) in the unit cell MBX$_3$. Based on the above formula, the obtained values of formation energy ΔE_F for these halide perovskites MBX$_3$ within the PBE-GGA calculations are summarized in (Table 4). As displayed in (Table 4), the values of formation energies ΔE_F for all these compounds are found to be negative. It is well known that chemical compound possessing smaller formation energy ΔE_F is more favorable in experimental synthesizing [42]. As a consequence, the obtained results of formation energy ΔE_F with small negative values indicate that all the compounds of halide perovskites MBX$_3$ are thermodynamically stable and can be synthesis experimentally in solid state phase according to the mechanochemical mixture (MX + BX$_2$ = MBX$_3$) [29,43].

Table 4. The calculated results of tolerance factor T_F, octahedral factor 0_F and formation energy ΔE_F per unit cell of MBX_3 (M^{1+} = Cs; B^{2+} = Si, Ge, Sn, Pb; X^- = Cl, Br, I).

MBX_3 compound	T_F	0_F %	ΔE_F (eV)
$CsSiCl_3$	1.129	38.32	−1.895
$CsSiBr_3$	1.104	35.16	−1.852
$CsSiI_3$	1.069	31.08	−1.786
$CsGeCl_3$	1.027	52.10	−1.720
$CsGeBr_3$	1.009	47.80	−1.675
$CsGeI_3$	1.009	42.23	−1.621
$CsSnCl_3$	1.019	53.29	−1.579
$CsSnBr_3$	0.998	48.90	−1.493
$CsSnI_3$	0.992	43.20	−1.481
$CsPbCl_3$	0.978	55.09	−1.452
$CsPbBr_3$	0.991	50.55	−1.438
$CsPbI_3$	1.007	44.66	−1.398

3.4. Electronic charge density

In the following subsections, we illustrate a comprehensive depiction for the electronic properties of the studied halide perovskites MBX_3 (M^{1+} = Cs; B^{2+} = Si, Ge, Sn, Pb; X^- = Cl, Br, I). The charge density, electronic band gaps, total density of states (TDOS) and partial density of states (PDOS) are calculated and discussed in detail.

First, in order to draw a deep insight into the electronic structures, the charge density in (100) plane of the unit cell for halide perovskites MBX_3 compounds is calculated by using the PBE-GGA method, and represented parallel with the crystal structures in Fig. 5. The 2D charge density plot and its contour lines allow visualizing the nature of the chemical bonds between the atoms in unit cell. Also, they elucidate the transfer mechanisms of charge carriers through these bonds. From the plot of 2D charge density for halide perovskites MBX_3 with (M^{1+} = Cs), (B^{2+} = Si, Ge, Sn, Pb) and X^- = Cl, Br, I), plus their corresponding partial density of states PDOSs that represented in Figs. 6-17, respectively, it can see that there are orbital hybridizations between the B^{2+}-p states of the cations Si^{2+}-3p Ge^{2+}-4p, Sn^{2+}-5p and Pb^{2+}-6p, and the anions X^--4p. The formation of these orbital hybridizations indicates that the nature of the chemical bonding between cations B^{2+} and anions X^- (B^{2+}–X^-) is the covalent bond, which confirmed by the condensed contour lines around both the ions of cations B^{2+} and anions X^- (Fig. 5). While, the form of other bonds, i.e. (M^{1+}–X^-) and (X^-–B^{2+}), show an ionic bond nature with minor contour lines. As a result, it is clear from all these 2D plots of charge density that the three ions of cation-anion bonds, M^{1+}, B^{2+} and X^-, in halide perovskites MBX_3 show a covalent-ionic mixture in their chemical bonding (M^{1+}–X^-) and (B^{2+}–X^-).

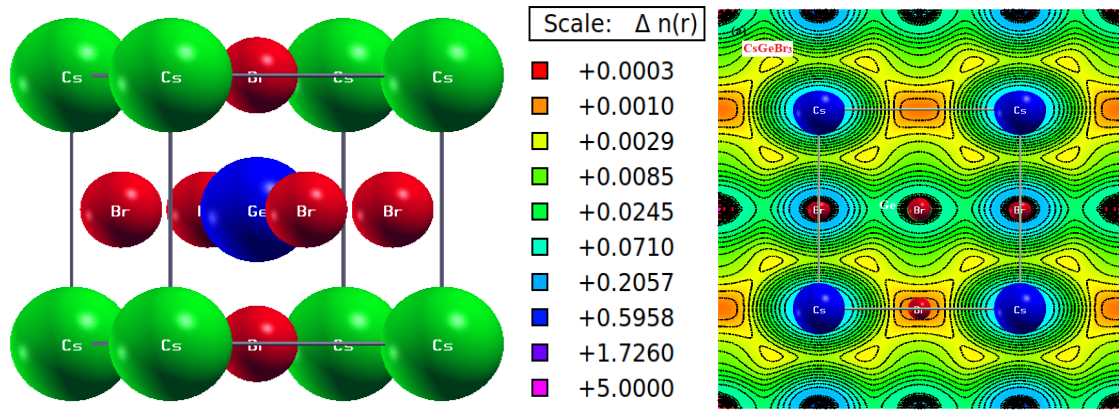*Fig. 5. The crystal structure and electronic charge density in (100) plane of the unit cells for the halide perovskite CsGeBr₃ in cubic symmetry (space group Pm-3m; No. 221) as example for MBX₃ (M¹⁺ = Cs; B²⁺ = Si, Ge, Sn, Pb; X⁻ = Cl, Br, I).*

3.5. Electronic band-gap

In order to study the main electronic features of halide perovskites MBX$_3$ (M^{1+} = Cs; B^{2+} = Si, Ge, Sn, Pb; X$^-$ = Cl, Br, I), the electric band gaps (E$_g$) are calculated using PBE-GGA method. They are extracted from the calculations of self consistent field (scf), along the high cubic symmetry points within the first Brillouin zone. Table 5 summarizes the calculated results of band gaps E$_g$ for the studied compounds MBX$_3$. These results enable us to compare and evaluate the differences in the values of band gaps (E$_g$) as a result of substituting the B^{2+} atom in the MBX$_3$ unit cells. The obtained results reveal that the PBE-GGA method gives band gaps E$_g$ very close to the previous results of experiments and DFT calculations [28-34]. As a consequence, all the cubic halide perovskites MBX$_3$ (M^{1+} = Cs; B^{2+} = Si, Ge, Sn, Pb) show semiconductor properties with direct band gaps E$_g$. also, by comparing the obtained results and examine the effect of substitution of B^{2+} atom, the band gap E$_g$ values as a function of B^{2+} atom, we can see that the core remark here, higher values of band gap E$_g$ are observed in the unit cell of halide perovskite MBX$_3$ with (B^{2+} = Pb) and then it decrease from (B^{2+} = Ge) to (B^{2+} = Sn) to (B^{2+} = Si) due to the increasing number and energy of total free electrons provide by B^{2+} atoms, Si: [Ne] 3s^2 3p^2, Ge: [Ar] 3d^{10} 4s^2 4p^2, Sn: [Kr] 4d^{10} 5s^2 5p^2 and Pb: [Xe] 5d^{10} 6s^2 6p^2, in conduction bands close to the Fermi level (E$_F$).

Table 5. The band gap (E$_g$) and equilibrium energy per unit cell of halide perovskites MBX$_3$ (M^{1+} = Cs; B^{2+} = Si, Ge, Sn, Pb; X$^-$ = Cl, Br, I).

MBX$_3$ compound	E$_g$ (eV)	E$_0$ (keV)
CsSiCl$_3$	0.557	-257.6
CsSiBr$_3$	0.635	-432.7
CsSiI$_3$	0.632	-801.0
CsGeCl$_3$	1.497	-306.8
CsGeBr$_3$	1.237	-481.9
CsGeI$_3$	1.120	-850.3
CsSnCl$_3$	1.367	-417.8
CsSnBr$_3$	1.071	-592.9
CsSnI$_3$	0.929	-961.3
CsPbCl$_3$	2.429	-819.2
CsPbBr$_3$	2.022	-994.3
CsPbI$_3$	1.736	-1362.6

3.6. Electronic density of states

Moreover, in order to evaluate the atomic contribution to the electronic total density of states TDOSs properties and the physical nature of atomic bonding for the compounds of halide perovskites MBX_3 (M^{1+} = Cs; B^{2+} = Si, Ge, Sn, Pb; X^- = Cl, Br, I), the following calculations of total density of states (TDOS) and partial density of states (PDOS) are performed using the PBE-GGA method, and plotted in Figs. 6-17. The first observation here, is that all TDOSs show an energy gap (E_g) around the E_F, with TDOS = 0.0 State/eV, which predict the semiconducting behavior of our MBX_3 perovskites. This prediction confirms the obtained PBE-GGA results from band structures in the previous subsection.

Table 5 summarizes the E_g values for MBX_3 compounds; the extending of their E_g significantly different with values ranging from E_g = 0.557 eV to 2.429 eV. Equivalent to that detected in band structures, the value of E_g increases also from B^{2+} = Si to B^{2+} = Ge to B^{2+} = Sn to B^{2+} = Pb due principally to the increasing number of energetic electrons of B^{2+} states in MBX_3. Practically, this prediction gives complete confidence of the tenability to develop such the proposed compounds as promising candidate materials for novel optoelectronic and photovoltaic technologies. Besides, since the value of E_g for the MBX_3 compounds can be simply tuned by applying the PBE-GGA method or through replacing the B^{2+}-site completely or partially by metalloid and post-transition atoms (B^{2+} = Si, Ge, Sn, Pb), the obtained semiconductor perovskites can also be exploited in the light-emitting diodes technology [37,44].

The second point, the PDOS curves, Figs. 6-17, confirm that the valence bands (VBs) of all MBX_3 compounds look similar and formed mainly by the hybridization of B^{2+}-s/p and X-p states, Si-3s/3p–X-p, Ge-4s/4p–X-p, Sn-5s/5p–X-p and Pb-6s/6p–X-p, appear between -5.0 eV and E_F. While their corresponding conduction bands (CBs) are generally dominated also by the hybridization of energetic 3p, 4p, 5p and 6p states in B^{2+}-p and X-p atoms. The top of the VBs beyond E_F is dominated mainly by partial B^{2+}-s and X-p electronic states, Si-3s–X-p, Ge-4s–X-p, Sn-5s–X-p and Pb-6s–X-p, whereas the bottom of CBs in the energy range in front of the E_F is majority occupied by B^{2+}-p states hybridize with tiny X-p, and there is no contribution come from Cs-5p and Cs-4d states, which locate after +3.50 eV away from E_F.
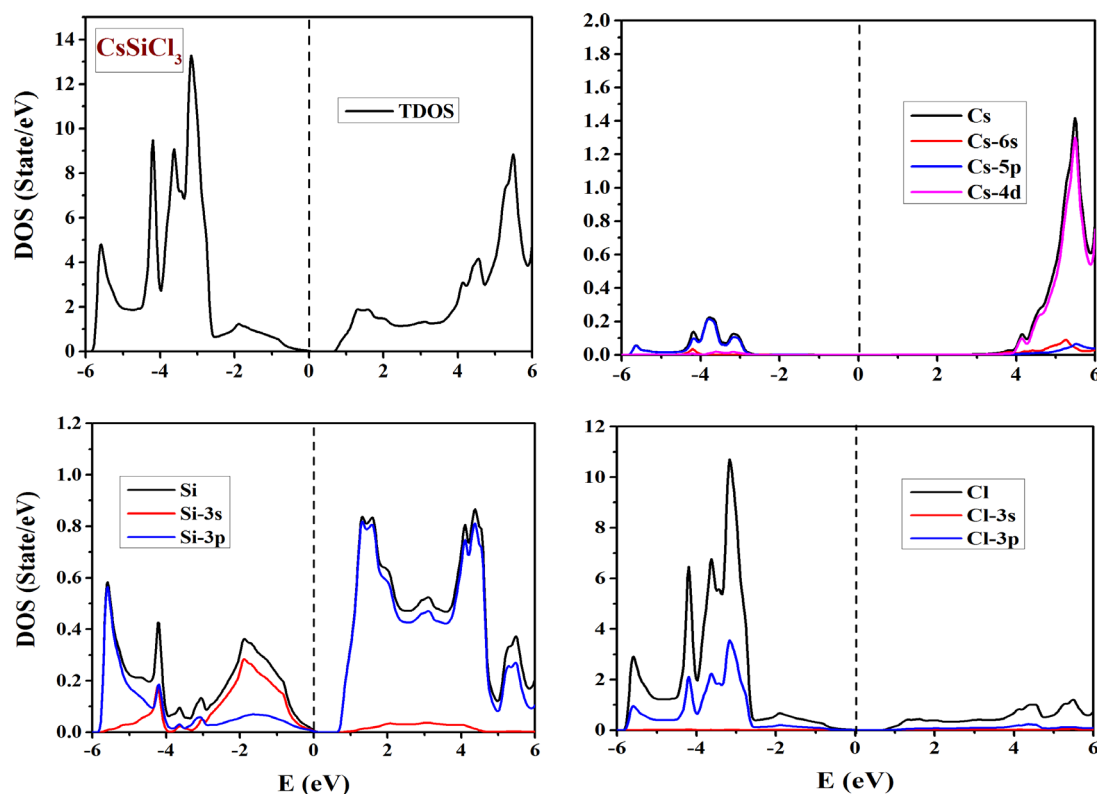

Fig. 6. The electronic TDOS per unit cell of CsSiCl₃ and its PDOS per atom of Cs, Si and Cl. The Fermi level (dash line) sets to zero (E_F = 0.0 eV).
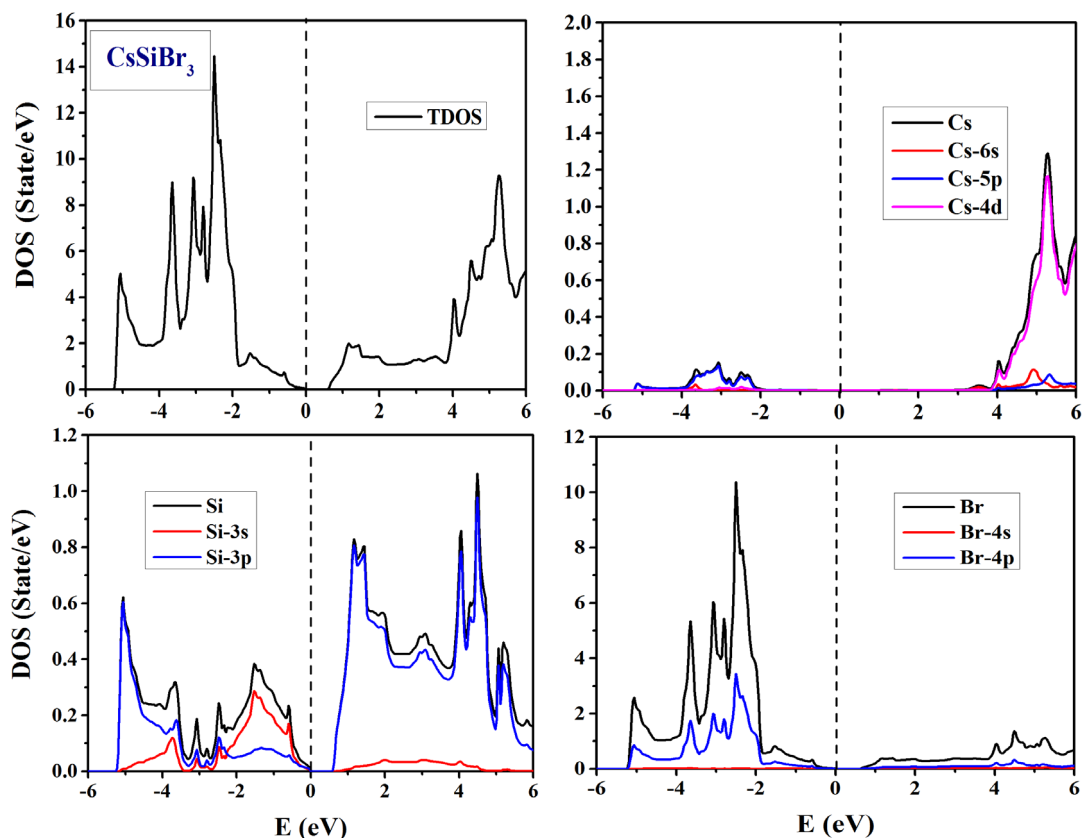
Fig. 7. The electronic TDOS per unit cell of CsSiBr$_3$ and its PDOS per atom of Cs, Si and Br. The Fermi level (dash line) sets to zero ($E_F = 0.0$ eV).
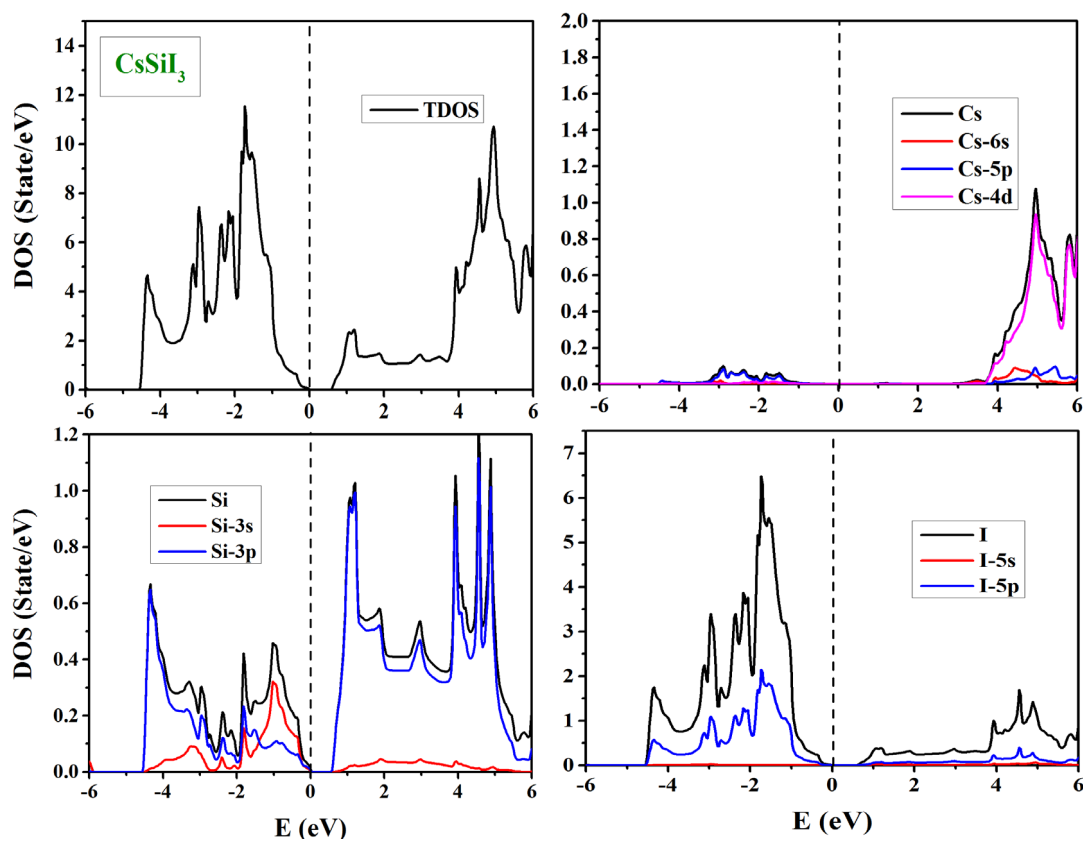

Fig. 8. The electronic TDOS per unit cell of CsSiI$_3$ and its PDOS per atom of Cs, Si and I. The Fermi level (dash line) sets to zero ($E_F = 0.0$ eV).

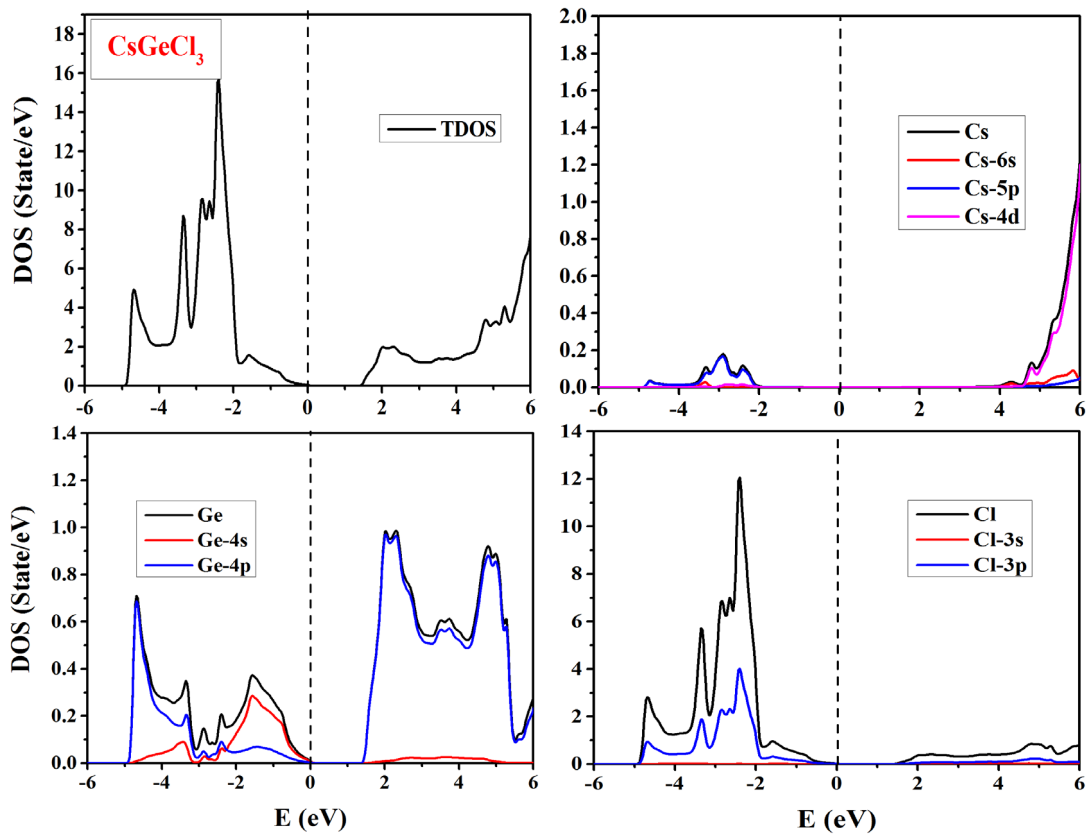*Fig. 9. The electronic TDOS per unit cell of CsGeCl$_3$ and its PDOS per atom of Cs, Ge and Cl. The Fermi level (dash line) sets to zero (E$_F$ = 0.0 eV).*
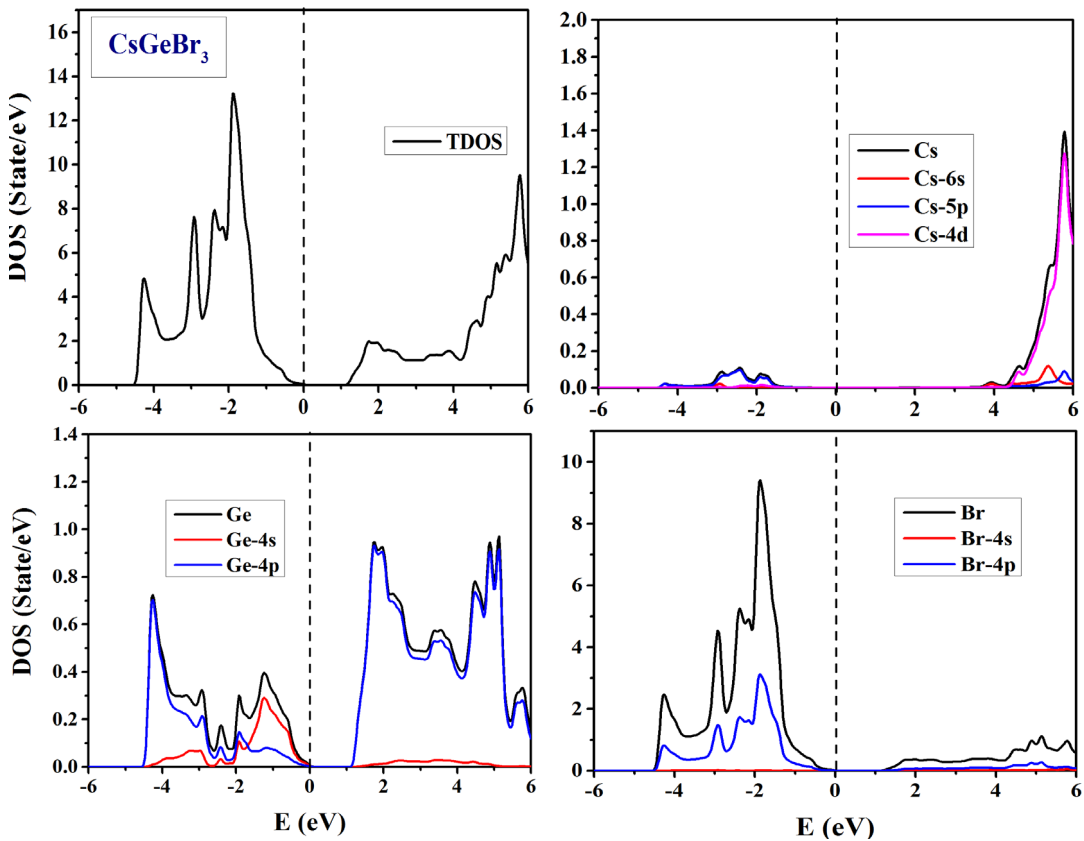

Fig. 10. The electronic TDOS per unit cell of CsGeBr$_3$ and its PDOS per atom of Cs, Ge and Br. The Fermi level (dash line) sets to zero (E$_F$ = 0.0 eV).
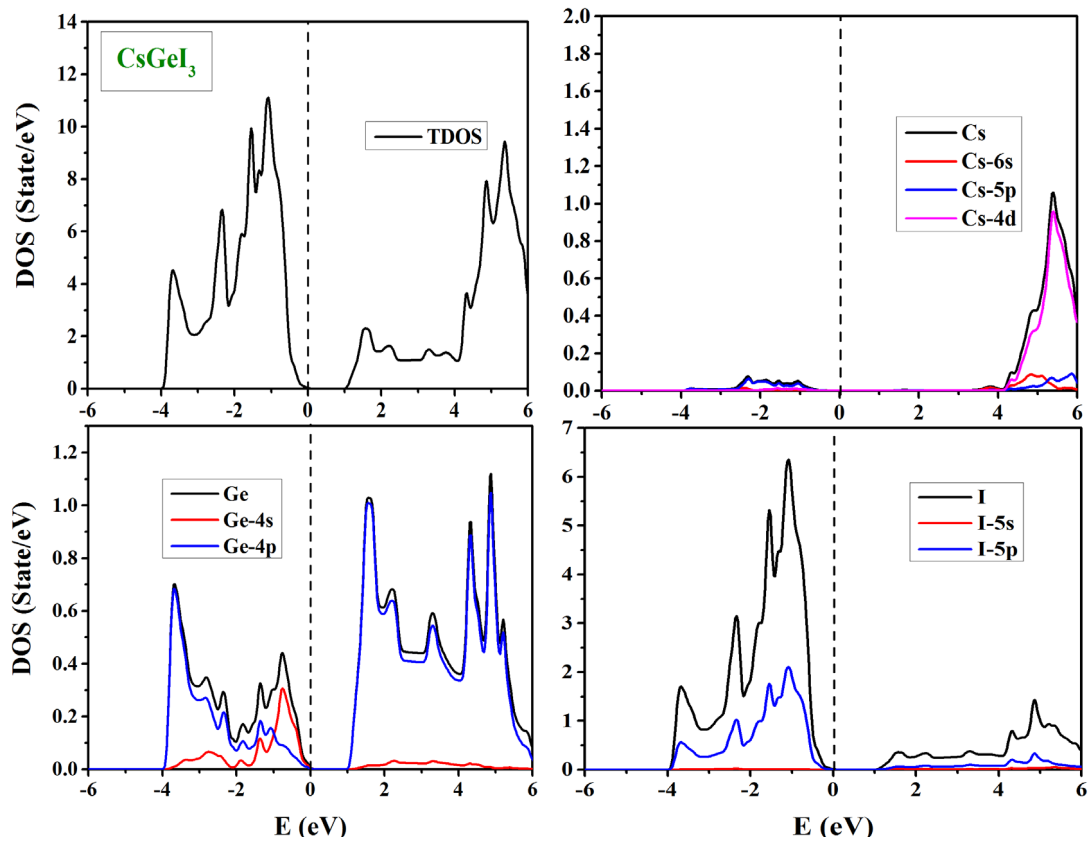
Fig. 11. The electronic TDOS per unit cell of CsGeI₃ and its PDOS per atom of Cs, Ge and I.
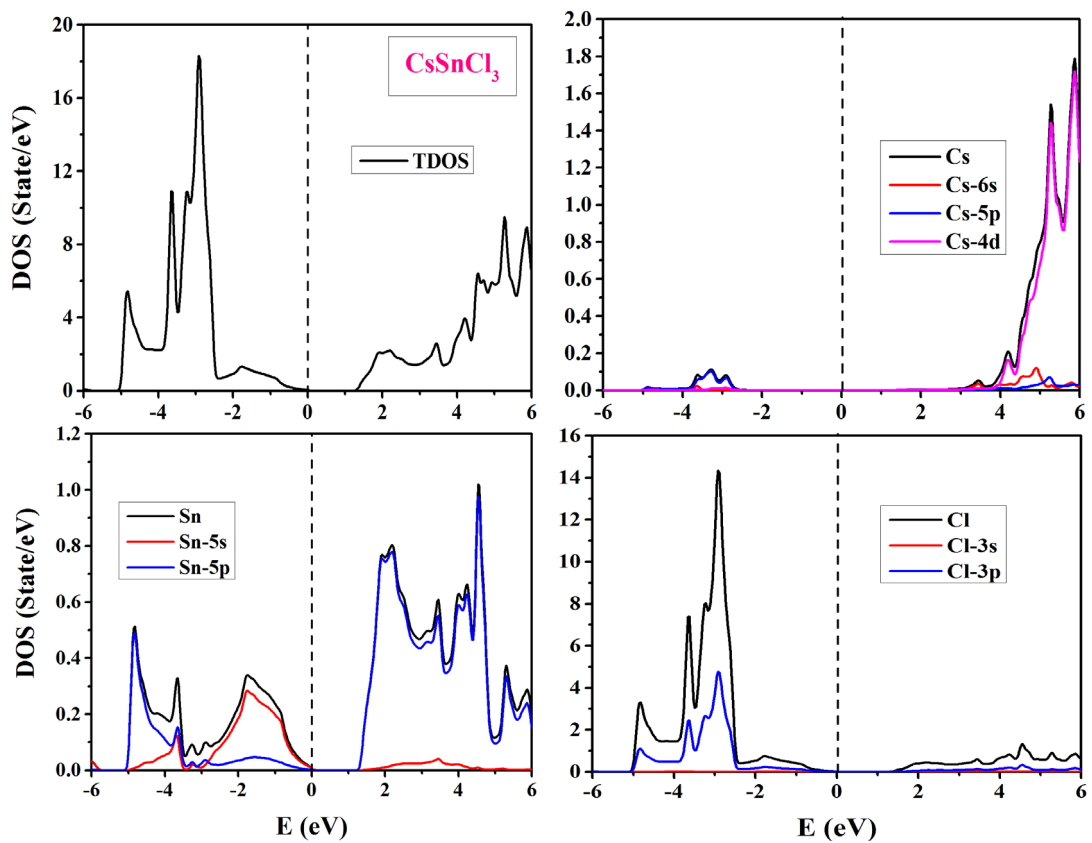The Fermi level (dash line) sets to zero ($E_F = 0.0$ eV).

Fig. 12. The electronic TDOS per unit cell of CsSnCl₃ and its PDOS per atom of Cs, Sn and Cl.
The Fermi level (dash line) sets to zero ($E_F = 0.0$ eV).
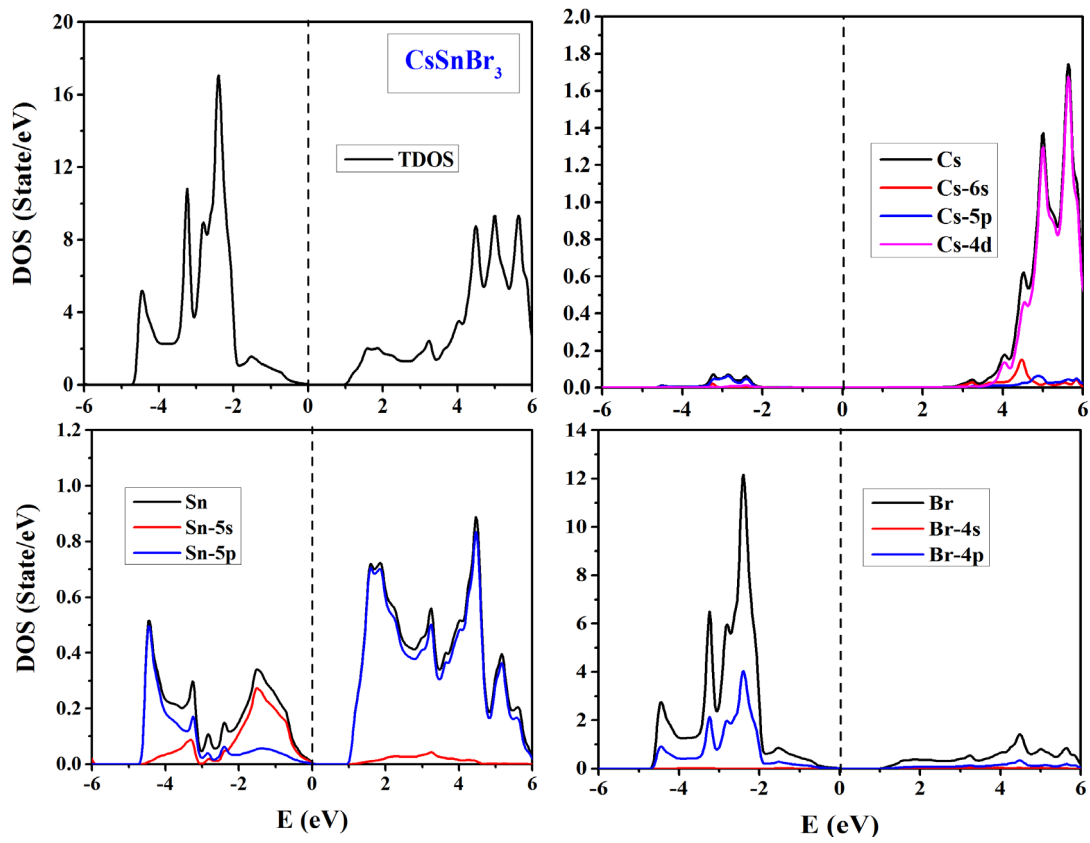
Fig. 13. The electronic TDOS per unit cell of CsSnBr₃ and its PDOS per atom of Cs, Sn and Br.
The Fermi level (dash line) sets to zero (E_F = 0.0 eV).

Fig. 14. The electronic TDOS per unit cell of CsSnI₃ and its PDOS per atom of Cs, Sn and I.
The Fermi level (dash line) sets to zero (E_F = 0.0 eV).

Fig. 15. The electronic TDOS per unit cell of CsPbCl₃ and its PDOS per atom of Cs, Pb and Cl.
The Fermi level (dash line) sets to zero (E_F = 0.0 eV).

Fig. 16. The electronic TDOS per unit cell of CsPbBr₃ and its PDOS per atom of Cs, Pb and Br.
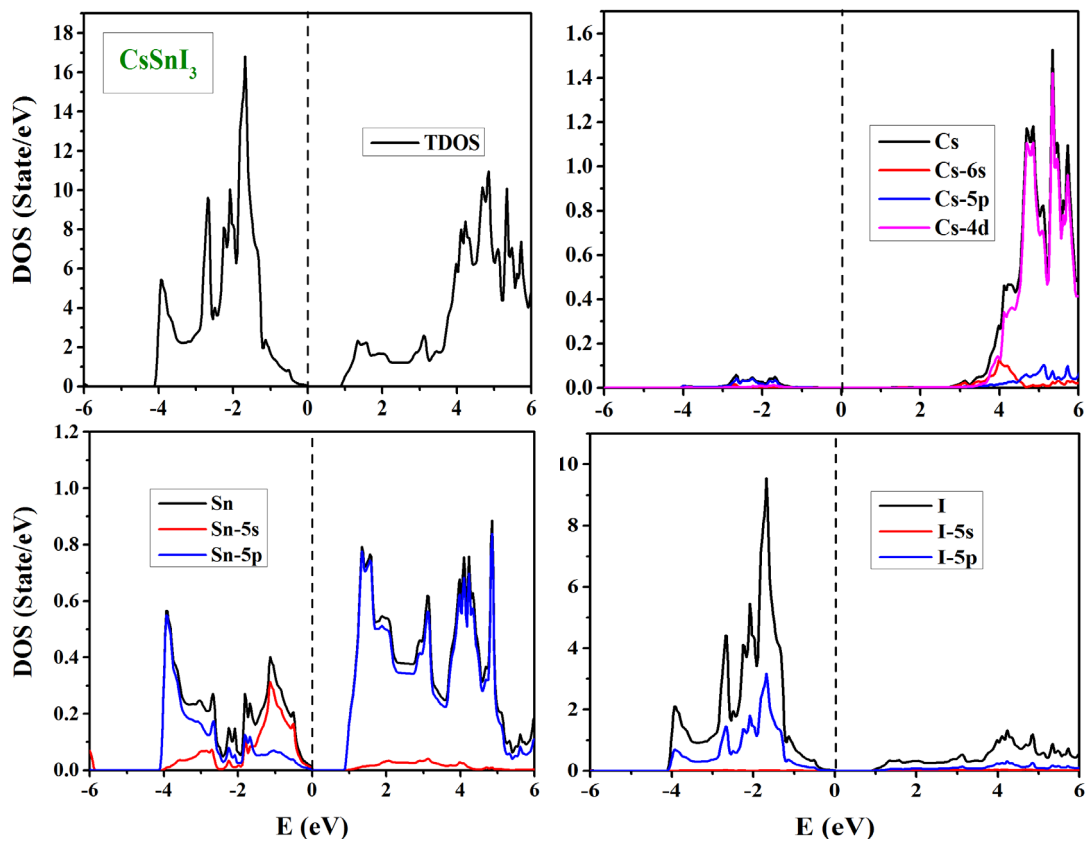*The Fermi level (dash line) sets to zero (E_F = 0.0 eV).*

Fig. 17. The electronic TDOS per unit cell of CsPbI₃ and its PDOS per atom of Cs, Pb and I.
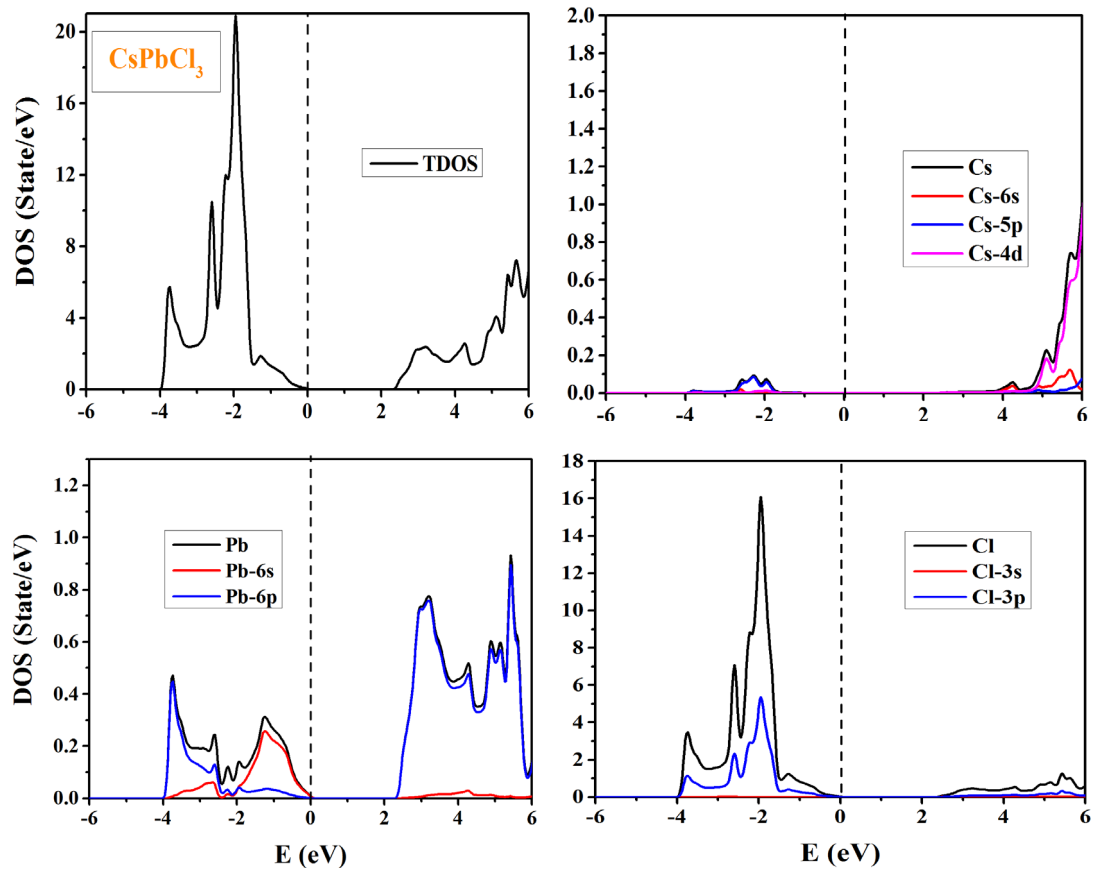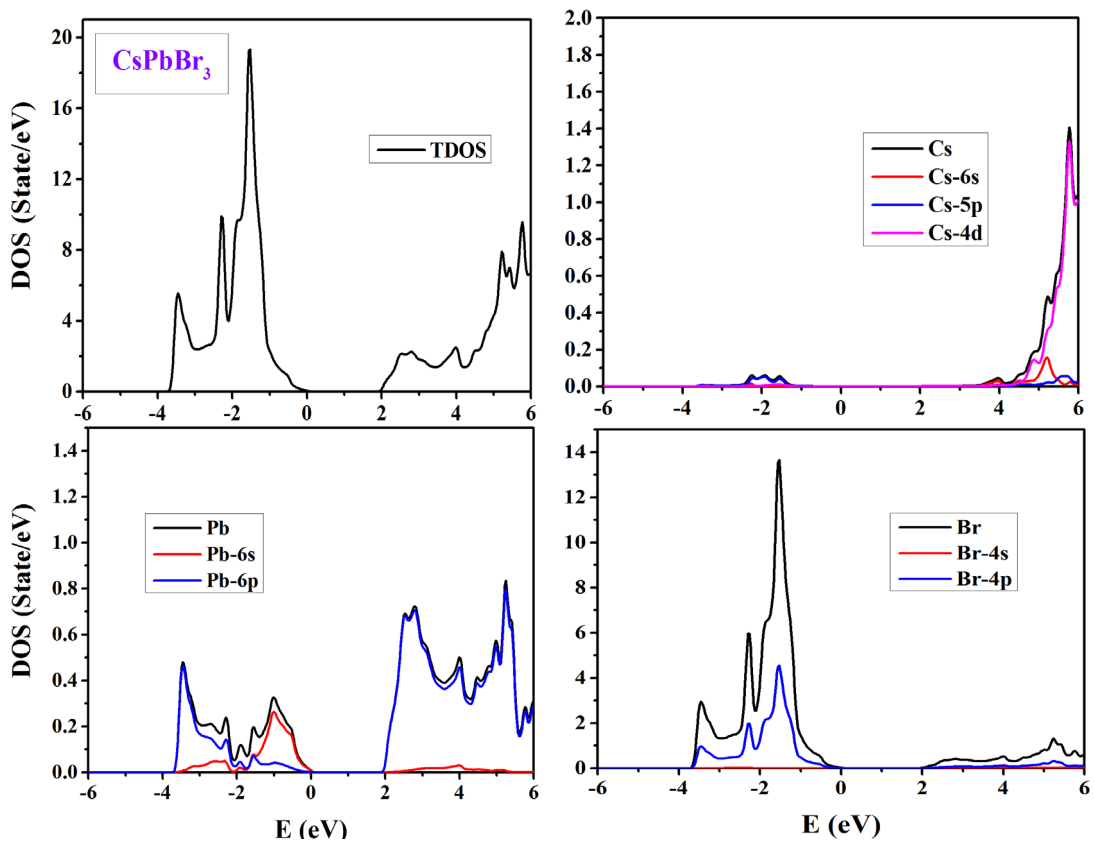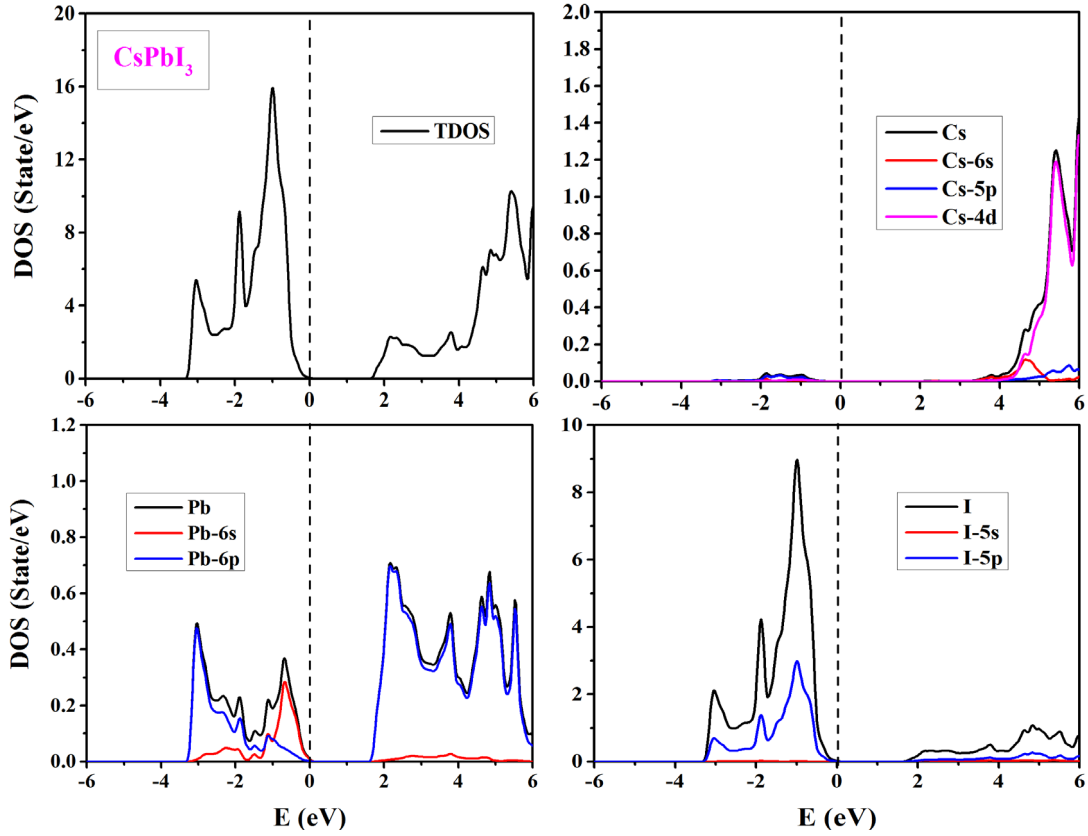*The Fermi level (dash line) sets to zero ($E_F = 0.0$ eV).*

3.7. Optoelectronic properties

As it is known that when high-energy light incidents on the surface of certain solid materials, a photoelectric interaction occurs between the crystal structures of these materials and photons of electromagnetic light. From the interaction outcomes it is possible to measure and quantify the photoresponse of materials. In this subsection, to evaluate this photoresponse and to obtain the main optical parameters, the optical properties of halide perovskites MBX_3 (M^{1+} = Cs; B^{2+} = Si, Ge, Sn, Pb; X^- = Cl, Br, I) are calculated. Herein, the details calculations of real part and imaginary part of the dielectric function, absorption coefficient, optical conductivity, refractive index, extinctive index, optical reflectivity and energy loss function have been carried out by using the PBE-GGA method. The results of optical parameters of MBX_3 compounds are represented in Figs. 18 (B^{2+} = Si), 19 (B^{2+} = Ge), 20 (B^{2+} = Sn) and 21 (B^{2+} = Pb), and discussed in detail. This examination is initiated by calculating the key optical parameter; i.e. the dielectric function (ε), as a function of the photon energy (ω) that can be described by the complex equation:

$$\varepsilon(\omega) = \varepsilon_1(\omega) + j\varepsilon_2(\omega) \qquad (5)$$

The Kramers-Kronig transformation (KKT) [38,39] expresses the real part $\varepsilon_1(\omega)$ and imaginary part $\varepsilon_2(\omega)$ of the dielectric function $\varepsilon(\omega)$ as:

$$\varepsilon_1(\omega) = 1 + \frac{2P}{\pi}\int_0^\infty \frac{\omega'\varepsilon_2(\omega')}{\omega'^2 - \omega^2}d\omega' \qquad (6)$$

$$\varepsilon_2(\omega) = \frac{8}{2\pi\omega^2}\sum_{nn'}|P_{nn'}(k)|^2\frac{dS_k}{\nabla\omega_{nn'}(\omega)} \qquad (7)$$

130

where, P = the principle part of integral, $\omega_{nn'}$ = energy difference between the energies ω and ω' of the states n and n', respectively, $P_{nn'}(k)$ = the electric-dipole matrix element between states n and n', and dS_k = the energy surface. However, dielectric function $\varepsilon(\omega)$ is defined as an energy tensor that leads to three components along the coordinates directions, x, y and z, and for cubic crystal structure, it is enough to calculate and study the optical parameters only along the x direction.

Based on the obtained values of real part $\varepsilon_1(\omega)$ and imaginary part $\varepsilon_2(\omega)$ of the dielectric function $\varepsilon(\omega)$, we can calculate the value of refractive index $N(\omega)$ as a sum of the real part $n(\omega)$ and imaginary part $k(\omega)$ of refractive index through the equations:

$$N(\omega) = [\varepsilon(\omega)]^{\frac{1}{2}} \tag{8}$$

$$N(\omega) = [\varepsilon_1(\omega) + j\varepsilon_2(\omega)]^{\frac{1}{2}} \tag{9}$$

$$N(\omega) = n(\omega) + jk(\omega) \tag{10}$$

The refractive index $n(\omega)$ and extinctive index $k(\omega)$ are respectively calculated using the following two equations:

$$n(\omega) = \left[\varepsilon_1(\omega) + \left(\frac{\varepsilon_1^2(\omega) + \varepsilon_2^2(\omega)}{4}\right)^{\frac{1}{2}}\right]^{\frac{1}{2}} \tag{11}$$

$$k(\omega) = \left[-\varepsilon_1(\omega) + \left(\frac{\varepsilon_1^2(\omega) + \varepsilon_2^2(\omega)}{4}\right)^{\frac{1}{2}}\right]^{\frac{1}{2}} \tag{12}$$

Using the value of extinctive index $k(\omega)$ and equation 12, the absorption coefficient $\alpha(\omega)$ can calculate using the equation:

$$\alpha(\omega) = 2\omega k(\omega) \tag{13}$$

$$\alpha(\omega) = \left[-\varepsilon_1(\omega) + 4\omega\left(\frac{\varepsilon_1^2(\omega) + \varepsilon_2^2(\omega)}{4}\right)^{\frac{1}{2}}\right]^{\frac{1}{2}} \tag{14}$$

The materials with very weakly optical absorbing have lesser value of absorption coefficient $\alpha(\omega)$. Then from equations 11, 12, 13 and 14, it can be expected that the value of extinctive index $k(\omega)$ is also very small, and this situation gives the values:

$$n(\omega) = [\varepsilon_1(\omega)]^{\frac{1}{2}} \tag{15}$$

$$k(\omega) = \frac{\varepsilon_2(\omega)}{2n(\omega)} \tag{16}$$

Furthermore, there are other important optical parameters; i.e. the reflection coefficient $R(\omega)$, which characterizes the part of energy reflected from the interface of the crystal structure. This coefficient can expressed using the values of refractive index $n(\omega)$ and extinctive index $k(\omega)$, as:

$$R(\omega) = \frac{[n(\omega) - 1]^2 + [k(\omega)]^2}{[n(\omega) + 1]^2 + [k(\omega)]^2} \tag{17}$$

Or by using the equation of dielectric function $\varepsilon(\omega)$:

$$R(\omega) = \left| \frac{[\varepsilon(\omega)]^{\frac{1}{2}} - 1}{[\varepsilon(\omega)]^{\frac{1}{2}} + 1} \right|^2 \qquad (18)$$

The optical conductivity $\sigma(\omega)$, equals to:

$$\sigma(\omega) = -j\frac{\omega}{4\pi}\varepsilon(\omega) \qquad (19)$$

$$\sigma(\omega) = \frac{\omega}{4\pi}\varepsilon_2(\omega) \qquad (20)$$

The static values of the important optical parameters such as real part of the dielectric function $\varepsilon_1(\omega)$ and refractive index $n(\omega)$ are listed in Table 6. They can be calculated at zero energy ($\omega = 0$), as:

$$n_s(0) = [\varepsilon_1(0)]^{\frac{1}{2}} \qquad (21)$$

In the following designs (Figs. 18-21) we plotted the calculated optical spectra as a function of photon energy $E(\omega)$ for the cubic halide perovskites MBX$_3$ (M^{1+} = Cs; B^{2+} = Si, Ge, Sn, Pb; X$^-$ = Cl, Br, I), respectively, where the variation in photon frequency (ω) is sketched in terms of energy range from (E = 0.0 eV to 15.0 eV). These spectra plots comprise the real part and imaginary part of dielectric function $\varepsilon(\omega)$, i.e. $\varepsilon_1(\omega)$ and $\varepsilon_2(\omega)$ respectively, the absorption coefficient $\alpha(\omega)$, the optical conductivity $\sigma(\omega)$, the refractive index $n(\omega)$, the extinctive index $k(\omega)$ and the optical reflectivity $R(\omega)$. Generally, it can clearly see that the X$^-$ atoms (X$^-$ = Cl, Br, I) give similar optical spectra for their corresponding compounds of halide perovskites MBX$_3$ with minor differences from the optical curves that obtained when (X$^-$ = Br).

First note, from the spectra of real part of the dielectric function $\varepsilon_1(\omega)$ for halide perovskites MBX$_3$ in (Figs. 18-21(a)), we can clearly see that there is an increase in the average values of the static dielectric function at zero energy ($\omega = 0$). Also, the positive curves of real part $\varepsilon_1(\omega)$ start from zero point with energy $\omega = 0$ and then increase to maximum values and final decrease with increasing in photonic energy ($\omega > 0$). While in high energy range, the real part $\varepsilon_1(\omega)$ curves decline to negative values. This means that the electromagnetic light are majority reflected from the medium of crystal structures of MBX$_3$ and their photon beam is totally reduced in this optical medium, which indicates that these crystal structures exhibit a metallic property in this photonic energy range. For that reason, these halide perovskites can be candidate materials for the protective shields against the electromagnetic light in the above specific energy range [28,34]. Within the energy range E = 0.0 eV to 10.10 eV, the substitution of B^{2+} atom through the series (B^{2+} = Si, Ge, Sn, Pb) does not affect the shape of optical curves as well as the values of real part $\varepsilon_1(\omega)$. While, for high values ($E(\omega) > 10\ eV$) the main peaks of real part $\varepsilon_1(\omega)$ are shifted to toward higher energy.

Compared the spectra of imaginary part of the dielectric function $\varepsilon_2(\omega)$ for MBX$_3$ compounds of halide perovskites MBX$_3$ in (Figs. 18-21 (b)) with their electronic dynamic in total densities of states TDOSs (Figs. 6-17), it can note that the behavior of spectrum for imaginary part $\varepsilon_2(\omega)$ characterize the absorptive power and they are closely linked with the electronic transitions from the occupied states in the valence bands (VBs) of M^{1+}, B^{2+} and X$^-$ crystal structures to unoccupied states in the conduction bands (CBs). Also, the edge values of imaginary part $\varepsilon_2(\omega)$ spectra for MBX$_3$ match well with the optical gaps of these compounds and are in complete agreement with the values of band gaps E$_g$ that obtained from the total densities of states TDOSs results (Table 5).

Second note, the spectra of optical conductivity $\sigma(\omega)$, as shown in (Figs. 18-21 (c)), stay constant at energy ($\omega = 0$) and then start to rise around energies correspond to the band gap E$_g$ values for all compounds of MBX$_3$, and then increase as the photon energy increases to form the

conductivity spectrum. The highest values of maximum conductivity $\sigma(\omega)$ is that of compounds with (B^{2+} = Si) and (B^{2+} = Ge) as a compared to other two ones, (B^{2+} = Sn) and (B^{2+} = Pb). The conductivity $\sigma(\omega)$ decreases as on move from (B^{2+} = Si to Ge to Sn and Pb) in MBX_3 compounds. However, all spectra involve four main peaks, which correspond to the small different transitions between symmetry points in the crystal structures of MBX_3, as they predicted in the electronic properties.

Third note, we plotted the corresponding photon energy dependent absorption spectra $\alpha(\omega)$, similar to conductivity $\sigma(\omega)$ spectra, for the compounds of halide perovskites MBX_3 in (Figs. 18-21(d)). Absorption parameter $\alpha(\omega)$ measures the electromagnetic light penetration through the crystal structures before it decaying totally. The values of absorption $\alpha(\omega)$ indicate that the optical absorption of the halide perovskite semiconductors MBX_3 are connected with the optoelectronic interactions occur between the photons of electromagnetic light and electrons in crystal structures. This because only the incident photons of light are responsible for the excitations of those electrons which carry high energy exceeding the values of band gaps E_g in their crystal structures, otherwise transmissions phenomena will occur through these crystal structures. It is clear that the absorption $\alpha(\omega)$ spectra of MBX_3 compounds show an increase of the absorption above the threshold frequency ($E(\omega) > E_g$), in the energy range (E = 2.0 eV – 14.0 eV) and then continuous to reach their maximum peaks due to the incoming photon light causing optoelectronic transitions. There are four step values of absorption $\alpha(\omega)$ spectra arise at certain energies. Consequently, the instant shift in imaginary part $\varepsilon_2(\omega)$ spectra represents the first direct optical transition and is equal to the optical gaps of MBX_3 compounds. The extending of these optical gaps closely relates to the detected values of band gaps E_g, signifying similar forms of the energy band contributions in the optoelectronic transitions. The optical gaps expand similarly within all compounds of MBX_3 as spotted from the semiconductor distributions of total densities of states TDOSs; however, the substitution of halide atom X^- X^- = Cl, Br, I) shows no significant variation than others. The crystal structures of MBX_3 show significant values of optical spectra of absorption $\alpha(\omega)$ among the range of Visible–UV light, however, the (B^{2+} = Ge) based crystal structures show highest absorption within the UV region (Table 6). Unfortunately, the absorption value decreases in (B^{2+} = Sn) and (B^{2+} = Pb) based crystal structures in the Visible as well as in UV range by small amount. Here, the predicted range of photon energy (E = 10 – 14 eV) agrees with the wavelength range ($\lambda \approx 916 - 1230$ Å) that belongs to the extreme UV light range, which make these compounds of halide perovskites MBX_3 promising materials for photoelectronics applications such as used in detectors, sensors and photoelectron spectroscopy [28,34,45]. The compounds of halide perovskites MBX_3 can be developed experimentally as thin-films solar cells materials since they have useful mechanical properties include high structural stability, high ductility and low elasticity. Furthermore, the wide range of energy for absorption $\alpha(\omega)$ spectra of MBX_3 that extends from Visible to UV domain, indicates the possibility of utilizing these compounds for various optoelectronics applications like photovoltaic solar cells, and physical detectors and sensors operating in Visible and UV range, respectively [34,46-48].

Fourth note, the refractive index $n(\omega)$ spectra for halide perovskites MBX_3 with (M^{1+} = Cs), (B^{2+} = Si, Ge, Sn, Pb) and (X^- = Cl, Br, I) are shown in (Figs. 18-21(e)), respectively. Also, the calculated and static values of refractive index n $n(0)$ are listed in (Table 6). From these spectra and results, it is clear that the values of calculated refractive index $n(0)$ and static refractive index $n_s(0)$ match exactly and increases slightly by utilizing the PBE-GGA method for all MBX_3 compounds. Conversely, the behavior of the extinctive index $k(\omega)$ as a function of the photon energy is shown in (Figs. 18-21(f)). Spectra of extinctive index $k(\omega)$ start around energy values correspond to the band gaps E_g, as for conductivity $\sigma(\omega)$ spectra, and then increase to reach their maximum values above (E = 11.0 eV). The real and imaginary parts of reflectivity spectra $R(\omega)$, which shown in (Figs. 18-21 (g)) and (Figs. 18-21 (h)), respectively, are consistent with the observed behavior of absorption $\alpha(\omega)$ spectra, the reflectivity $R(\omega)$ decreases in the sequence (B^{2+} = Si, Ge, Sn, Pb) for MBX_3 with (M^{1+} = Cs) and (X^- = Cl, Br, I). The maximum values of reflectivity $R(\omega)$ correspond to the negative values of real part of the dielectric function $\varepsilon_1(\omega)$ at the range ($E(\omega) > 10\ eV$), where the percentages of reflectivity $R(\omega)$ for these crystal structures are found to be nearly similar and about 56.5%, 50.4% and 50.3%, respectively, within PBE-GGA

method. The calculated and static values of various optical parameters for MBX_3 (B^{2+} = Si, Ge, Sn, Pb) at zero energy ($\omega = 0$), as well as the estimation of their key optical absorption $\alpha(\omega)$ and optical conductivity $\sigma(\omega)$, are listed in (Table 6). The increase of absorption $\alpha(\omega)$ spectra at around (E = 1.0 eV – 3.0 eV) indicates the application of solar light within the VL–UV range, and this nature is very beneficial for photovoltaics PV, solar cells and optoelectronics technology.

Table 6. The maximum values of real part $\varepsilon_1(\omega)$ and refractive index $n(\omega)$ at zero energy ($\omega = 0$), the static values $n_s(0)$ are calculated using equation (21), for halide perovskites MBX_3 (M^{1+} = Cs; B^{2+} = Si, Ge, Sn, Pb; X^- = Cl, Br, I). Also, the evaluation of the key optical properties for the absorption $\alpha(\omega)$ and conductivity $\sigma(\omega)$, (H = High, M = Medium and L = Less).

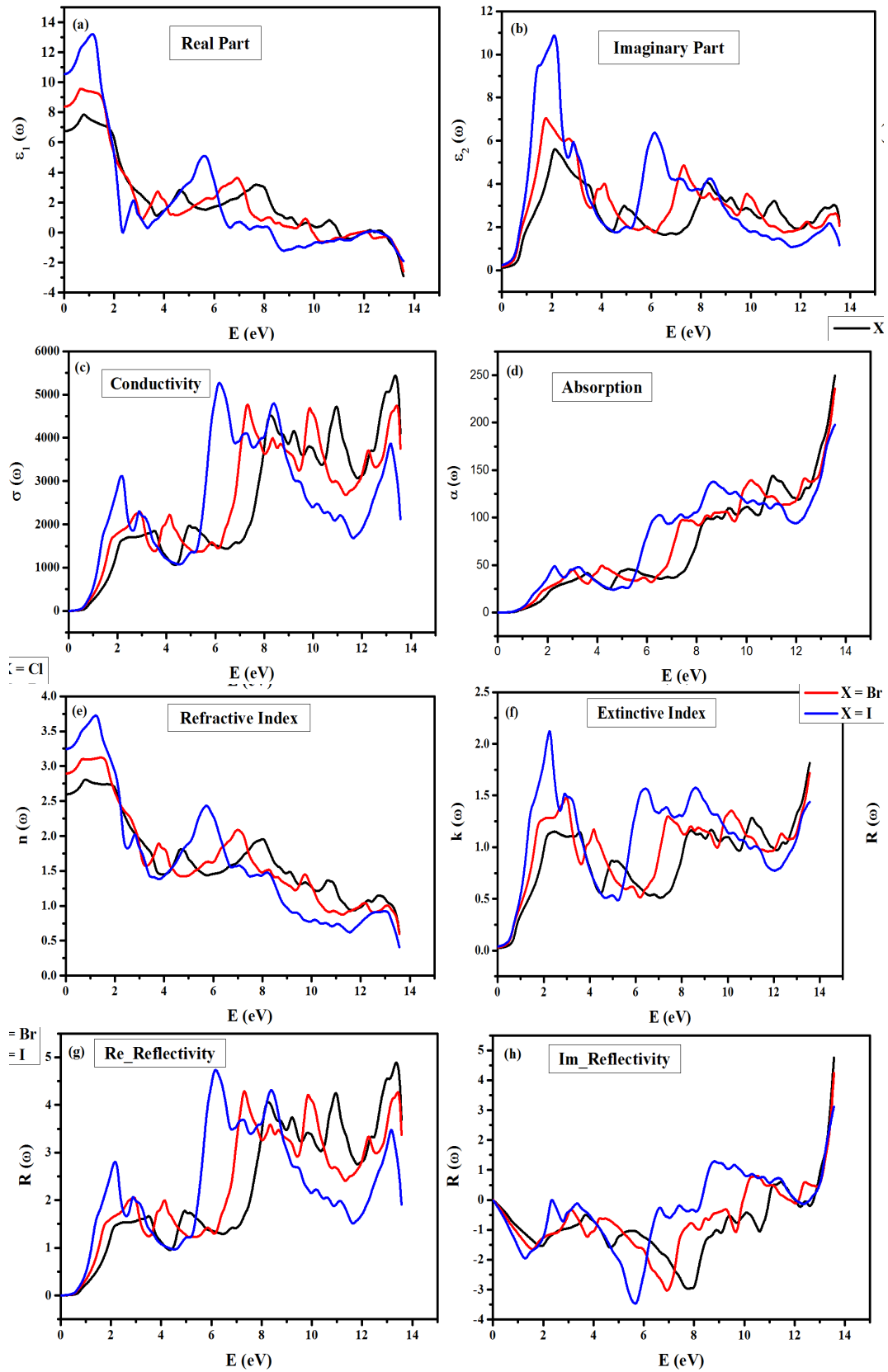| MBX_3 compound	$\varepsilon_1(0)$	$n(0)$	$n_s(0)$	$\alpha(\omega)$	$\sigma(\omega)$
$CsSiCl_3$	6.746	2.599	2.597	H	M
$CsSiBr_3$	8.377	2.896	2.894	H	M
$CsSiI_3$	10.54	3.249	3.247	H	M
$CsGeCl_3$	4.928	2.220	2.220	H	M
$CsGeBr_3$	6.142	2.478	2.478	H	M
$CsGeI_3$	8.160	2.857	2.857	H	M
$CsSnCl_3$	4.474	2.115	2.115	M	L
$CsSnBr_3$	5.595	2.366	2.365	M	L
$CsSnI_3$	7.204	2.685	2.684	M	L
$CsPbCl_3$	3.497	1.870	1.870	L	L
$CsPbBr_3$	4.260	2.064	2.064	L	L
$CsPbI_3$	5.484	2.342	2.342	L	L

134

Fig. 18. The photon energy-dependent parameters: (a) real part of dielectric function $\varepsilon_1(\omega)$, (b) imaginary part of dielectric function $\varepsilon_2(\omega)$, (c) optical conductivity $\sigma(\omega)$, (d) absorption coefficient $\alpha(\omega)$, (e) refractive index $n(\omega)$, (f) extinctive index $k(\omega)$, (g) real reflectivity $R(\omega)$ and (h) imaginary reflectivity $R(\omega)$ of halide perovskites $CsSiX_3$ ($X = Cl, Br, I$).

Fig. 19. The photon energy-dependent parameters: (a) real part of dielectric function $\varepsilon_1(\omega)$, (b) imaginary part of dielectric function $\varepsilon_2(\omega)$, (c) optical conductivity $\sigma(\omega)$, (d) absorption coefficient $\alpha(\omega)$, (e) refractive index $n(\omega)$, (f) extinctive index $k(\omega)$, (g) real reflectivity $R(\omega)$ and (h) imaginary reflectivity $R(\omega)$ of halide perovskites $CsGeX_3$ ($X^- = Cl$, Br, I).
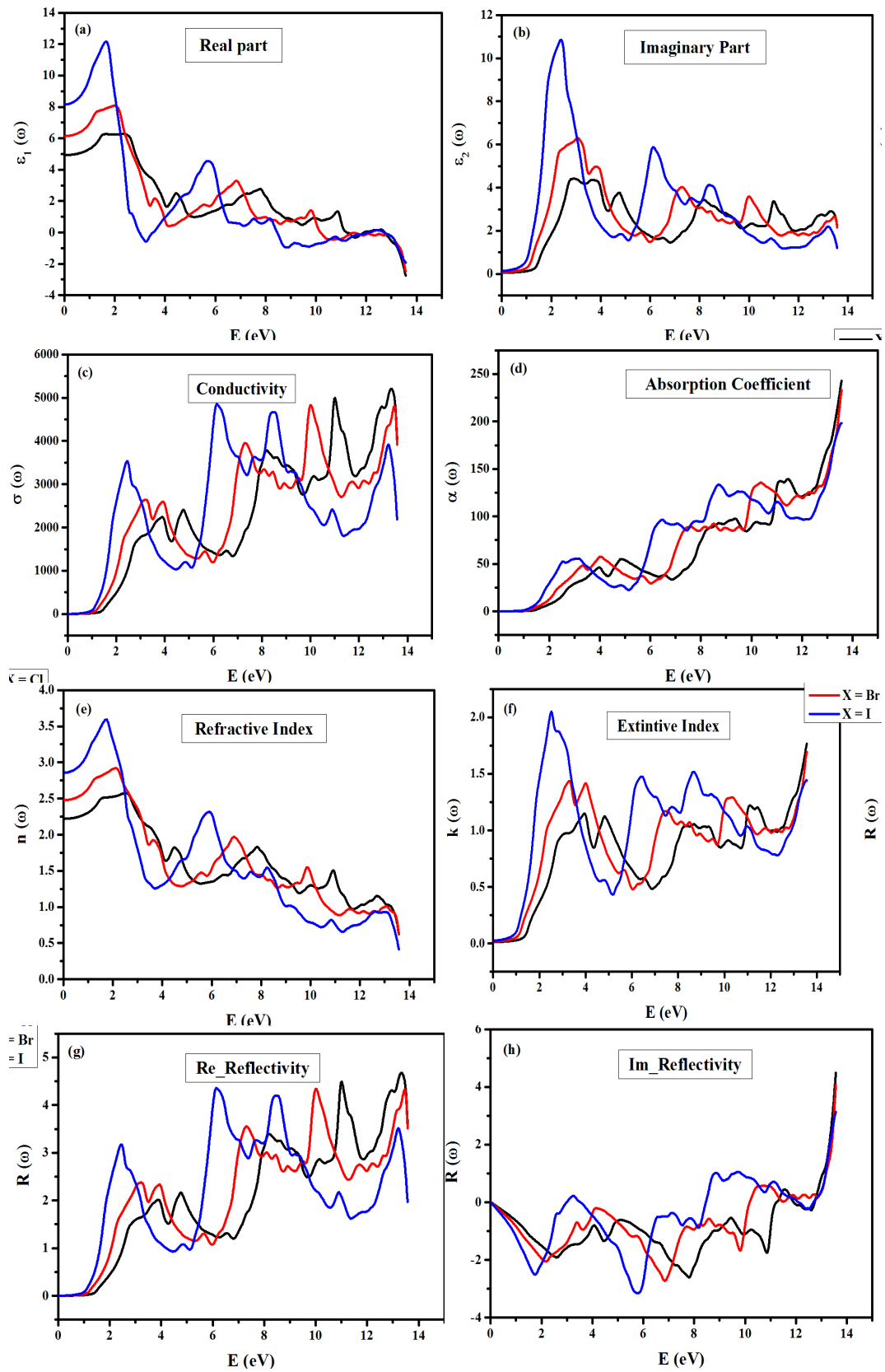
Fig. 20. The photon energy-dependent parameters: (a) real part of dielectric function $\varepsilon_1(\omega)$, (b) imaginary part of dielectric function $\varepsilon_2(\omega)$, (c) optical conductivity $\sigma(\omega)$, (d) absorption coefficient $\alpha(\omega)$, (e) refractive index $n(\omega)$, (f) extinctive index $k(\omega)$, (g) real reflectivity $R(\omega)$ and (h) imaginary reflectivity $R(\omega)$ of halide perovskites $CsSnX_3$ ($X^- = Cl, Br, I$).
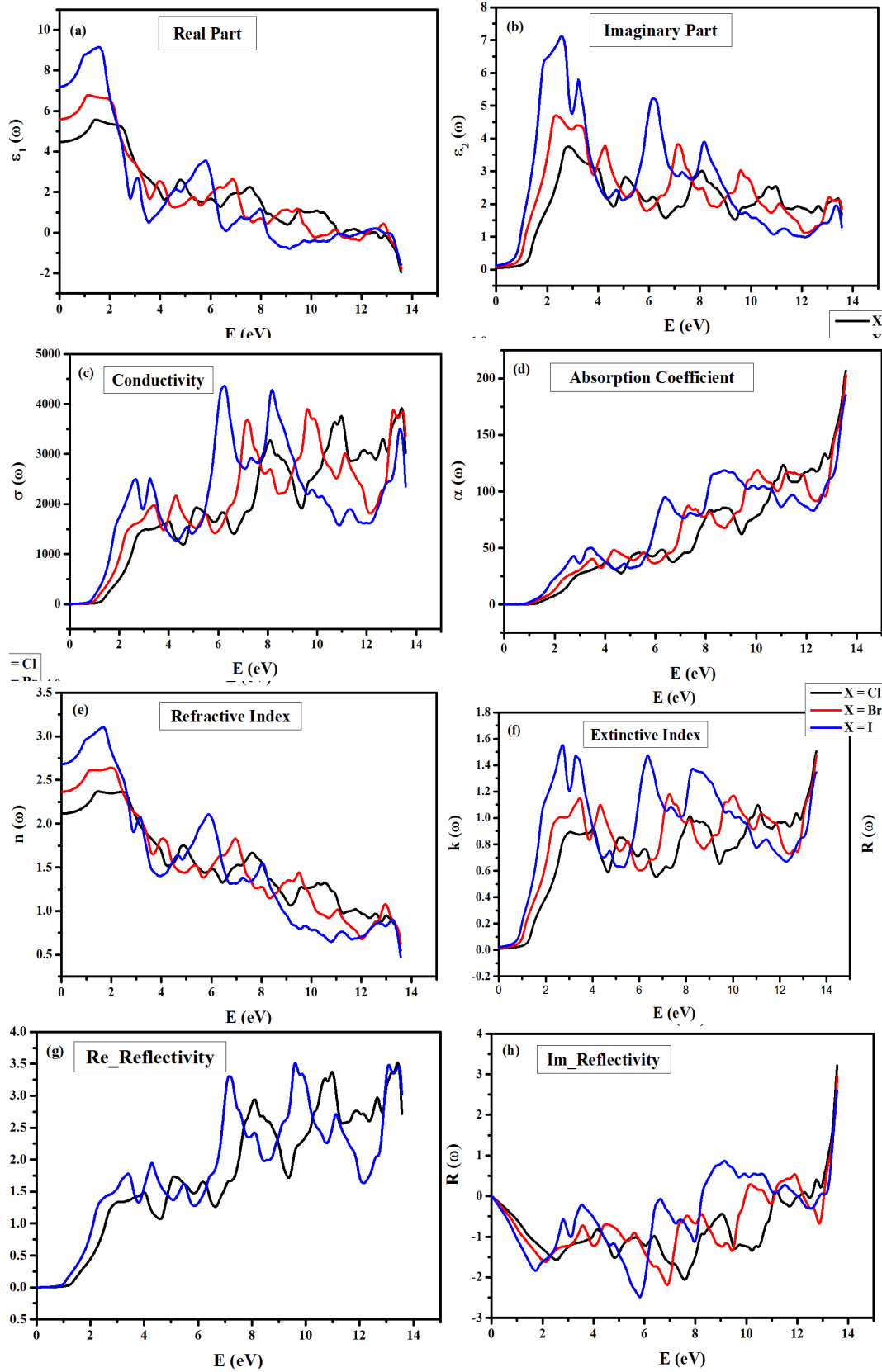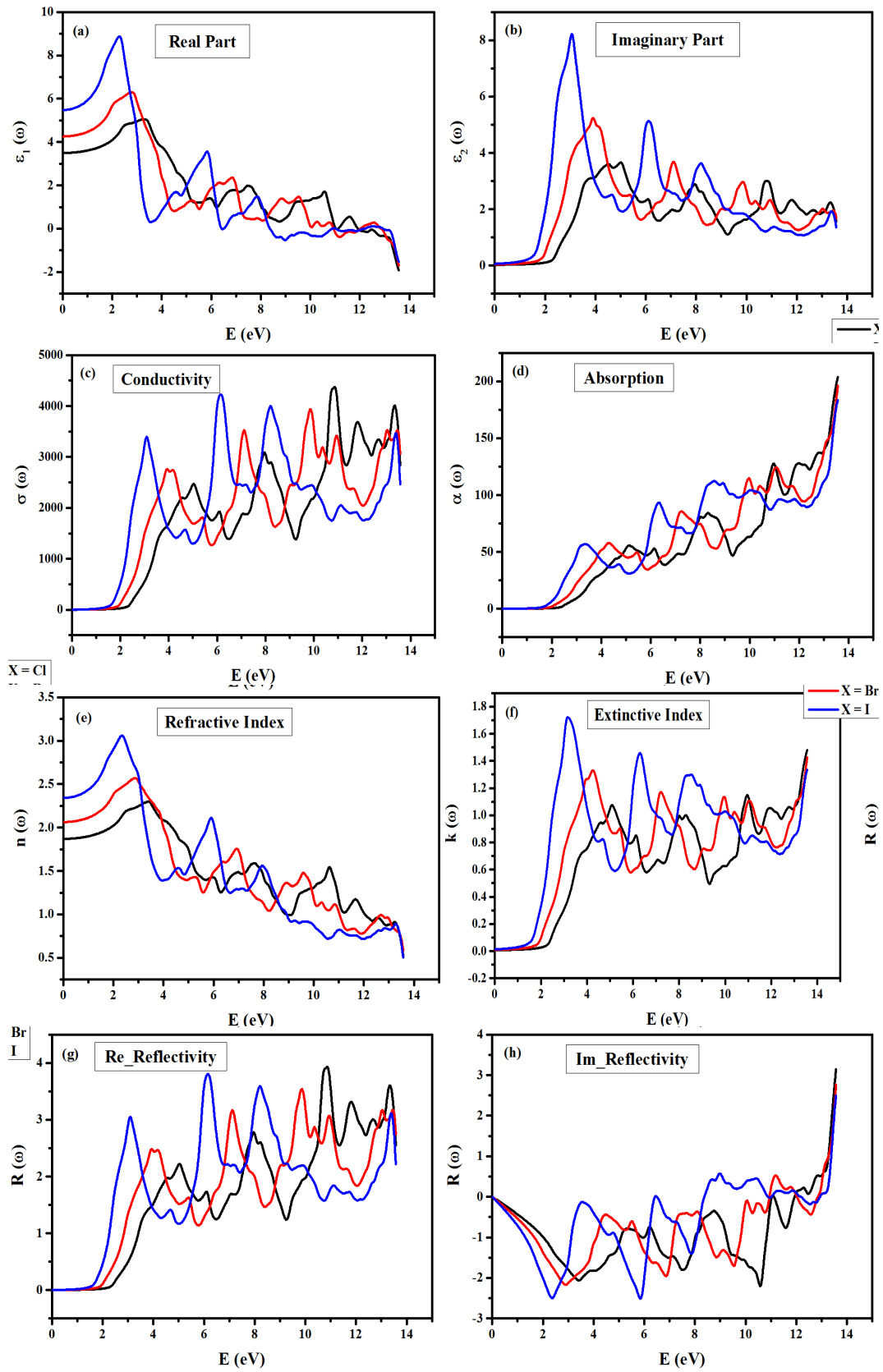
Fig. 21. The photon energy-dependent parameters: (a) real part of dielectric function $\varepsilon_1(\omega)$, *(b) imaginary part of dielectric function* $\varepsilon_2(\omega)$, *(c) optical conductivity* $\sigma(\omega)$, *(d) absorption coefficient* $\alpha(\omega)$, *(e) refractive index* $n(\omega)$, *(f) extinctive index* $k(\omega)$, *(g) real reflectivity* $R(\omega)$ *and (h) imaginary reflectivity* $R(\omega)$ *of halide perovskites* $CsPbX_3$ *(X⁻ = Cl, Br, I).*

4. Conclusions

In this study, we have performed a detailed investigation on the structural, electronic and optical properties of cesium-metalloid halide perovskites MBX_3 with (M^{1+} = Cs; B^{2+} = Si, Ge, Sn, Pb; X^- = Cl, Br, I). Density functional theory (DFT) calculations based on the FPLAPW method are carried out. The method PBE within the generalized gradient approximation (GGA) has been used in all calculations. The optimized and calculated results of crystal structures show stability properties of the cubic structure (Pm-3m; No. 221) for the studied compounds. The results of calculated density of states by PBE-GGA method show that the present halide perovskites MBX_3 with (M^{1+} = Cs), (B^{2+} = Si, Ge, Sn, Pb) and (X^- = Cl, Br, I) exhibit nonmagnetic phase and semiconductor properties with proper band gaps. The obtained results show the dependence of value for these band gaps E_g essentially on the variation of B^{2+} atom, allowing easily modifying and tuning the value of band gap E_g by applying this technique to be useful in possible applications of tunable optoelectronics and photovoltaic PV solar cells.

Moreover, the calculated optical spectra by PBE-GGA method reveal that the crystal structures of MBX_3 have good optical absorption and conductivity, and the (B^{2+} = Si) and (B^{2+} = Ge) based halide perovskites show higher values than the compounds with (B^{2+} = Sn) and (B^{2+} = Pb). In addition to the mechanical stability of halide perovskites MBX_3 and their suitable values of direct band gap E_g, the wide range of optical absorption, which matches to the energy within the Visible–UV light range, indicates the possibility of using these halide perovskites MBX_3 for the flexible optoelectronics applications, such as photovoltaic PV solar cells, photodetectors, photodiodes and other photovoltaic PV devices operating in this range of electromagnetic light. Finally, we advise that the studied compounds of halide perovskites MBX_3 (M^{1+} = Cs; B^{2+} = Si, Ge, Sn, Pb; X^- = Cl, Br, I) can be synthesized as thin films solar cells materials due to their functional properties.

References

[1] Z. Shi, A. H. Jayatissa, Materials 11, 729 (2018); https://doi.org/10.3390/ma11050729

[2] M. A. Green, K. Emery, Y. Hishikawa, W. Warta, E. D. Dunlop, Prog. Photovoltaics Res. Appl. 20, 606 (2012); https://doi.org/10.1002/pip.2267

[3] J. Even, L. Pedesseau, E. Tea, S. Almosni, A. Rolland, C. Robert, J.-M. Jancu, C. Cornet, C. Katan, J.-F. Guillemoles, O. Durand, Int. J. Photoenergy 649408 (2014); https://doi.org/10.1155/2014/649408

[4] F. Alrashed, M. Asif, Energy Proced. 18, 1096 (2012); https://doi.org/10.1016/j.egypro.2012.05.124

[5] Y. Ye, X. Run, X. H.-Tao, H. Feng, X. Fei, W. L.-Jun, Chin. Phys. B 24, 116302 (2015).

[6] L. Sánchez, J. A. D. Pascual, A. M. Capilla, R. Peña, Int. J. Mol. Sci. 20, 976 (2019); https://doi.org/10.3390/ijms20040976

[7] F. Deschler, D. Neher, L. S. Mende, APL Mater. 7, 080401 (2019); https://doi.org/10.1063/1.5119744

[8] A. K. Chilvery, A. K. Batra, B. Yang, K. Xiao, P. Guggilla, M. D. Aggarwal, R. Surabhi, R. B. Lal, J. R. Currie, B. G. Penn, J. Photon. Energy 5, 057402 (2015); https://doi.org/10.1117/1.JPE.5.057402

[9] G. Lozano, J. Phys. Chem. Lett. 9, 3987 (2018); https://doi.org/10.1021/acs.jpclett.8b01417

[10] M. Pazoki, T. Edvinsson, Sustainable Energy Fuels 2, 1430 (2018); https://doi.org/10.1039/C8SE00143J

[11] S. Yun, Y. Qin, A. R. Uhl, N. Vlachopoulos, M. Yin, D. Li, X. Han, A. Hagfeldt, Energy Environ. Sci. 11, 476 (2018); https://doi.org/10.1039/C7EE03165C

[12] B. Cai, X. Chen, M. Xie, S. Zhang, X. Liu, J. Yang, W. Zhou, S. Guo, H. Zeng, Mater. Horiz. 5, 961 (2018); https://doi.org/10.1039/C8MH00590G

[13] N. Kumar, J. Rani, R. Kurchania, Mater. Today-Proc. 46(11), 5570 (2021);

https://doi.org/10.1016/j.matpr.2020.09.349

[14] V. Jella, S. Ippili, J.-H. Eom, S. V. N. Pammi, J.-S. Jung, V.-D. Tran, V. H. Nguyen, A. Kirakosyan, S. Yun, D. Kim, M. R. Sihn, J. Choi, Y.-J. Kim, H.-J. Kim, S.-G. Yoon, Nano Energy 57, 74 (2019); https://doi.org/10.1016/j.nanoen.2018.12.038

[15] W. Xiang, W. Tress, Advanced Materials 31, 1902851 (2019); https://doi.org/10.1002/adma.201902851

[16] Q. Zhang, Y. Yin, ACS Cent. Sci. 4(6), 668 (2018); https://doi.org/10.1021/acscentsci.8b00201

[17] D. B. Raja, K. S. Sundaram, R. Vidya, Solar Energy 207, 1348 (2020); https://doi.org/10.1016/j.solener.2020.07.044

[18] L. M. Herz, ACS Energy Lett. 2 (7), (2017), 1539; https://doi.org/10.1021/acsenergylett.7b00276

[19] T. I. Mohammed, S. C. L. Koh, I. M. Reaney, A. Acquaye, G. Schileo, K. B. Mustapha, R. Greenough, Renew. Sust. Energy Rev. 80, 1321 (2017); https://doi.org/10.1016/j.rser.2017.05.095

[20] A. Zhang, Y. Chen, J. Yan, IEEE J. Quantum Elect. 52(6), (2016); https://doi.org/10.1109/JQE.2016.2563783

[21] P. Hohenberg, W. Kohn, Phys. Rev. 136(3B), 864 (1964); https://doi.org/10.1103/PhysRev.136.B864

[22] K.H. Schwarz, P. Blaha, G. K. H. Madsen, Comput. Phys. Commun. 147, 71 (2002); https://doi.org/10.1016/S0010-4655(02)00206-0

[23] W. Kohn, L.J. Sham, Phys. Rev. 140 A, 1133 (1965); https://doi.org/10.1103/PhysRev.140.A1133

[24] J. P. Perdew, K. Burke, M. Ernzerhof, Phys. Rev. Lett. 77, 3865 (1996); https://doi.org/10.1103/PhysRevLett.77.3865

[25] J. P. Perdew, A. Ruzsinszky, G. I. Csonka, O. A. Vydrov, G. E. Scuseria, L. A. Constantin, X. Zhou, K. Burke, Phys. Rev. Lett. 100, 136406 (2008); https://doi.org/10.1103/PhysRevLett.100.136406

[26] Z. Wu, R. E. Cohen, Phys. Rev. B 73, 235116 (2006); https://doi.org/10.1103/PhysRevB.73.235116

[27] L. C. Tang, J. Y. Huang, C. S. Chang, M. H. Lee, L. Q. Liu, J. Phys.: Condens. Matter 17, 7275 (2005); https://doi.org/10.1088/0953-8984/17/46/011

[28] M. A. Islam, M. Z. Rahaman, S. K. Sen, AIP Adv. 11, 075109 (2021); https://doi.org/10.1063/5.0057287

[29] M. Houari, B. Bouadjemi, S. Haid, M. Matougui, T. Lantri, Z. Aziz, S. Bentata, B. Bouhafs, Indian J. Phys. 94, 455 (2020); https://doi.org/10.1007/s12648-019-01480-0

[30] U. Schwarz, H. Hillebrecht, M. Kaupp, K. Syassen, H.-G. Schnering, G. Thiele, J. Solid State Chem. 118, 20 (1995); https://doi.org/10.1006/jssc.1995.1305

[31] W. J. Shi, J. Liu, Y. Xu, S. J. Xiong, J. Wu, W. Duan, Phys. Rev. B 92, 205118 (2015); https://doi.org/10.1103/PhysRevB.92.205118

[32] L. Peedikakkandya, P. Bhargava, RSC Adv. 6, 19857 (2016); https://doi.org/10.1039/C5RA22317B

[33] M. Roknuzzaman, K. K. Ostrikov, H. Wang, A. Du, T. Tesfamichael, Sci. Rep. 7, 14025 (2017); https://doi.org/10.1038/s41598-017-13172-y

[34] H. M. Ghaithan, Z. A. Alahmed, S. M. H. Qaid, M. Hezam, A. S. Aldwayyan, ACS Omega 5, 7468 (2020); https://doi.org/10.1021/acsomega.0c00197

[35] V. M. Goldschmidt, D. G. Krystallochemie, D. Naturwiss. 14, 477 (1926); https://doi.org/10.1007/BF01507527

[36] R. D. Shannon, Acta Cryst. A 32, 751 (1976); https://doi.org/10.1107/S0567739476001551

[37] S. G. Kang, J. Solid State Chem. 262, 251 (2018); https://doi.org/10.1016/j.jssc.2018.03.026

[38] S. Chen, T. Bimenyimana, M. Guli, Results Phys. 14, 102408 (2019); https://doi.org/10.1016/j.rinp.2019.102408

[39] M. Boubchir, H. Aourag, Comput. Condens. Matter 24, e00495 (2020); https://doi.org/10.1016/j.cocom.2020.e00495

[40] S. Safari, S. M. S. Ahmadian, A. R. Ghadim, J. Photoch. Photobio. A 394, 112461 (2020); https://doi.org/10.1016/j.jphotochem.2020.112461

[41] W. Travis, E. N. K. Glover, H. Bronstein, D. O. Scanlon, R. G. Palgrave, Chem. Sci. 7, 4548 (2016); https://doi.org/10.1039/C5SC04845A

[42] L. Zhou, J. Chang, Z. Lin, C. Zhang, D. Chen, J. Zhang, Y. Hao, RSC Adv. 7, 54586 (2017); https://doi.org/10.1039/C7RA11514H

[43] E. Aleksanyan, A. Aprahamian2, A. S. Mukasyan, V. Harutyunyan, K. V. Manukyan, J. Mater. Sci. 55, 8665 (2020); https://doi.org/10.1007/s10853-020-04617-3

[44] K. Ji, M. Anaya, A. Abfalterer, S. D. Stranks, Adv. Optical Mater. 2002128 (2021); https://doi.org/10.1002/adom.202002128

[45] D. Menzel, A. Tejada, A. Al-Ashouri, I. Levine, J. A. Guerra, B. Rech, S. Albrecht, L. Korte, ACS Appl. Mater. Interfaces 13, 43540 (2021); https://doi.org/10.1021/acsami.1c10171

[46] W. J. Yin, J.H. Yang, J. Kang, Y. Yan, S. H. Wei, J. Mater. Chem. A 3, 8926 (2015); https://doi.org/10.1039/C4TA05033A

[47] A. N. El-Shazly, M. Y. Rezk, K. M. Gameel, N. K. Allam, ACS Appl. Nano Mater. 2, 7085 (2019); https://doi.org/10.1021/acsanm.9b01613

[48] J. Hao, Y.-H. Kim, S. N. Habisreutinger, S. P. Harvey, E. M. Miller, S. M. Foradori, M. S. Arnold, Z. Song, Y. Yan, J. M. Luther, J. L. Blackburn, Sci. Adv. 7, eabf1959 (2021); https://doi.org/10.1126/sciadv.abf1959